


Review

Metal-Organic Frameworks as a Platform for CO₂ Capture and Chemical Processes: Adsorption, Membrane Separation, Catalytic-Conversion, and Electrochemical Reduction of CO₂

Salma Ehab Mohamed Elhenawy ¹, Majeda Khraisheh ^{1,*}, Fares AlMomani ¹ and Gavin Walker ²

¹ Department of Chemical Engineering, College of Engineering, Qatar University, Doha P.O. Box 2713, Qatar; se1105821@student.qu.edu.qa (S.E.M.E.); falmomani@qu.edu.qa (F.A.)

² Bernal Institute, Department of Chemical Sciences, University of Limerick, V94 T9PX Limerick, Ireland; Gavin.Walker@ul.ie

* Correspondence: m.khraisheh@qu.edu.qa; Tel.: +974-4403-4990 (ext. 4138); Fax: +974-4403-4001

Received: 17 September 2020; Accepted: 28 October 2020; Published: 9 November 2020



Abstract: The continuous rise in the atmospheric concentration of carbon dioxide gas (CO₂) is of significant global concern. Several methodologies and technologies are proposed and applied by the industries to mitigate the emissions of CO₂ into the atmosphere. This review article offers a large number of studies that aim to capture, convert, or reduce CO₂ by using a superb porous class of materials (metal-organic frameworks, MOFs), aiming to tackle this worldwide issue. MOFs possess several remarkable features ranging from high surface area and porosity to functionality and morphology. As a result of these unique features, MOFs were selected as the main class of porous material in this review article. MOFs act as an ideal candidate for the CO₂ capture process. The main approaches for capturing CO₂ are pre-combustion capture, post-combustion capture, and oxy-fuel combustion capture. The applications of MOFs in the carbon capture processes were extensively overviewed. In addition, the applications of MOFs in the adsorption, membrane separation, catalytic conversion, and electrochemical reduction processes of CO₂ were also studied in order to provide new practical and efficient techniques for CO₂ mitigation.

Keywords: metal organic frame works; CO₂ adsorption; pre combustion; gas membrane separation

1. Introduction

The Earth's global climate system is continually facing devastating changes due to various human-made and natural factors. Smithson [1] mentioned that the increase in greenhouse gas concentrations in the atmosphere directly impacts the global climate system, which is known as global warming [1]. These greenhouse gases trap the sun's radiation in the Earth's atmosphere; this phenomenon is known as the greenhouse effect, causing global warming. Carbon dioxide gas is blamed for being the main factor that causes the greenhouse effect because it is the most important anthropogenic greenhouse gas (Intergovernmental Panel on Climate Change (IPCC), 2007) [2]. Rochelle [3] stated that more than 85% of the world's energy demand is based on burning fossil fuels; this will result in massive emissions of CO₂ into the atmosphere [3]. There are natural and anthropogenic sources for carbon dioxide gas emissions into the atmosphere. Chemical engineering industries are considered one of the primary anthropogenic sources of CO₂ into the atmosphere in which natural gas and fossil fuels are burned for various purposes. As a result of the industrial revolution and the rapid increase in the population growth rate, more fossil fuels are burnt to satisfy

the population's needs and demands. Hence, more carbon dioxide is emitted into the atmosphere. Consequently, the separation and capture of CO₂ became a necessity.

CO₂ can be separated and captured using five leading technologies, including absorption, adsorption, cryogenics, membrane, and microbial or algae [4]. In the meantime, the research trend has been focusing on three main types of technology for carbon capture, namely oxy-fuel combustion, pre-combustion, and post-combustion. Omoregbe (2020) investigated those main types of technology by using publications retrieved from the Web of Science database from the year 1998 to 2018. The results of the authors' investigations presented that from the year 1998 to 2007 there was almost no research output on carbon capture, until the year 2008, in which climate change abatement was first introduced, and the industrial and public awareness of clean, greener fossil energy options grew. The authors also stated that among the commonly studied carbon capture technologies, the post-combustion capture technology was the most referenced technology for carbon capture, with approximately 80.9% of total publications retrieved. On the other hand, the technology with the lowest number of publications is oxy-fuel combustion, with approximately 3.4% of total publications retrieved [5]. Several porous materials can be incorporated into these carbon capture technologies to allow and enhance the separation or the capture of CO₂. One of the best-used porous materials in carbon capture technologies are metal-organic frameworks (MOFs).

During the last two decades, a new crystalline porous materials class has emerged [6]. This class of materials is known as MOFs. As a result of the MOFs' unique properties, this class has gained remarkable attention across the globe. The main limitation of the application of MOFs in the carbon capture processes is the high cost. The synthesis process of MOFs is very costly, which makes them economically unviable. This review paper investigates MOFs' applications in the CO₂ capture, adsorption, separation, conversion, and reduction processes. It aims to draw and provide general guidelines and conclusions for the MOFs' importance as a porous material for carbon dioxide gas-related process.

2. Fundamentals of Metal-Organic Frameworks (MOFs)

MOFs are made-up of metal-containing nodes linked by organic ligand bridges and assembled primarily by strong coordination bonds; this can be shown in Figure 1 below. MOFs have well defined crystallographic and geometric three-dimensional (3D) microporous structures [7]. These structures are sturdy and durable, allowing the removal of the included guest species, which results in permanent porosity.

MOFs can be easily designed, synthesized, and tuned. By comparing MOFs to other porous materials like zeolites and activated carbons, MOFs allows a facile optimization of the structures of their pores, surface functions, and other properties, making them applicable for several specific and precise applications as porous materials. MOFs can be categorized into two classes flexible/dynamic [8] and rigid. Flexible MOFs hold a dynamic and soft framework with a fast response to external stimuli, for example, guest molecules, temperature, and pressure. This extraordinary and superb sensitivity to external stimuli allows the MOFs to possess special properties such as temperature/pressure-dependent molecular sieving, which puts them ahead of the traditional adsorbents, including activated carbons and zeolites.

On the other hand, rigid MOFs possess a stable and strong porous framework with an enduring porosity that is similar to zeolites. In the meantime, rigid MOFs have been used extensively for the selective gas adsorption processes. The selective adsorption mechanism in rigid MOFs is quite similar to zeolites; hence selective adsorption can be achieved based on the molecular sieving effect. Also, it is probably achieved according to the strength of the different interactions between adsorbate–adsorbate and adsorbate–adsorbent. Li, et al. [9] mentioned that selective adsorption in rigid MOFs depends on three main factors: adsorbate–surface interactions, size/shape exclusion, and simultaneous corporation of both factors.

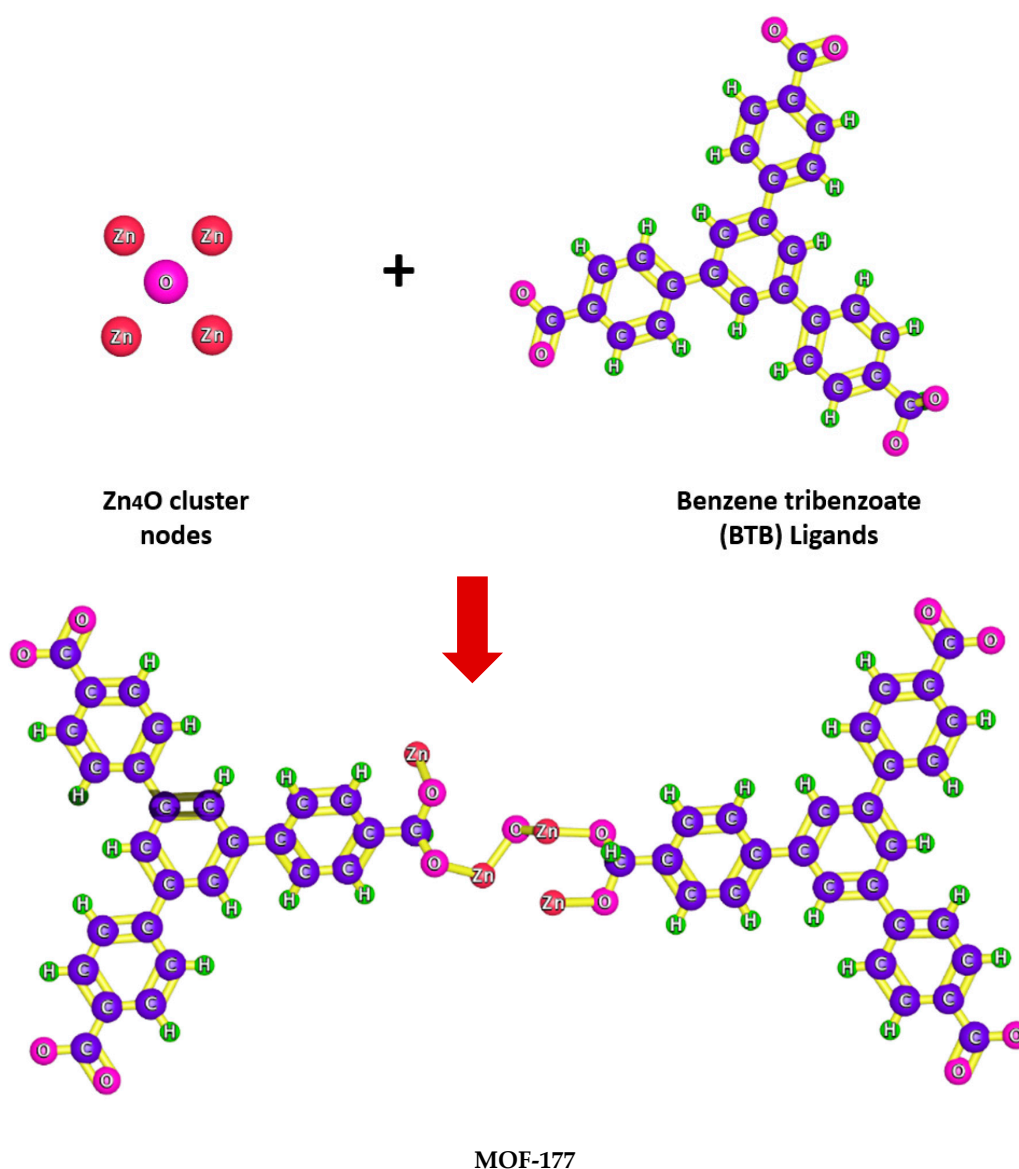


Figure 1. Typical synthesis approach for metal-organic framework MOF-177.

Based on the literature, many MOFs are used to selectively adsorb different gases relying on the molecular sieving effect [10–13]. This implies that only the molecules with appropriate pore kinetic diameters can pass through the MOF pores (Figure 2). Table 1 below shows the kinetic diameters of several gases.

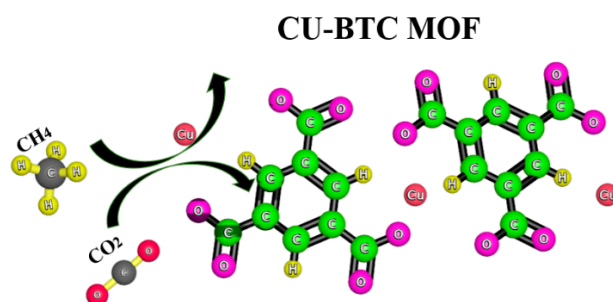


Figure 2. Schematic diagram of selective gas adsorption in Cu-BTC MOF (copper benzene-1,3,5-tricarboxylate) based on molecular sieving effect.

Table 1. Kinetic diameters of several gases [14].

Molecule	Kinetic Diameter (Å)
CO ₂	3.3
O ₂	3.46
N ₂	3.64
H ₂ O	2.65
CH ₄	3.8
H ₂	2.89

MOFs can be synthesized with an exceptionally high porosity under mild conditions via self-assembly reaction between organic linkers and several metal ions. Table 2 below provides chemical formulas and chemical structures of some organic ligands in some frequently used MOFs.

Table 2. Chemical formulas and chemical structures of some organic ligands in some frequently used MOFs [15].

MOF Name	Organic Ligand	Organic Ligand Structure
MOF-200	BBC: 4,4',4''-benzene-1,3,5-triyl-tris(benzene-4,1-diyl)tribenzoate	
MOF-177	BTB: 4,4',4''-benzene-1,3,5-triyl-tribenzoate	
MOF-180	BTE: 4,4',4''-benzene-1,3,5-triyl-tris(ethyne-2,1-diyl)tribenzoate	
MOF-205	BTB + 2,6-naphthalenedicarboxylate (NDC)	
MOF-210	BTE + biphenyl-4,4'-dicarboxylate (BPDC)	

In the field of porous materials, MOFs have excelled and surpassed the traditional porous materials in the following properties: they possess very high CO₂ [16] and methane storage [17], uptake of hydrogen-based on physical adsorption [18], and surface area [19]. Hence, MOFs are extensively used in the carbon capture processes. Table 3 below shows a comparison between the strengths and weaknesses of carbon capture materials. It can be seen from Table 3 that MOFs have the highest working capacity among all other carbon capture materials.

Table 3. Strengths and weaknesses comparison of selected carbon-capture materials [20].

	MOFs	Liquid Amines	Amine Grafted MOFs	Zeolites	Ionic Liquids	Hybrid Ultraporos Materials (HUMs)	Soda Lime	Amine Grafted Inorganics
Selectivity	Low	High	High	Low	High	Very high	High	High
Stability	Low	Low	Medium	High	High	Medium	High	High
Humidity effect	High	Low	Medium	High	Low	Medium	Low	Low
Material cost	Medium/high	Low	High	Low	Low	Low	Low	Medium
Process cost	Medium	Low	High	Low	Medium	Low	Low	Medium
Recycling cost	High	High	Medium	High	Medium/high	Low	Very high	Medium
Working capacity	High	Medium	Medium	Medium	Low	Medium	Medium	Medium
Kinetics	Medium	Fast	Medium	Medium	Fast	Fast	Fast	Medium
Upside potential	High	Low	Medium	Low	Medium	High	Low	Medium

An extensive number of review articles have been published recently to highlight the extreme developments in the synthesis, design, and application of MOFs in the carbon dioxide capture and storage (CCS) field [21–23]. Simmons, et al. [24] stated that MOFs had been displayed as excellent materials for carbon dioxide storage, and also they are useful in the removal of carbon dioxide from flue gas stacks [24]. MOFs can be consequently considered ideal membrane-filling materials and adsorbents for CO₂ gas storage, separation, and capture due to their pore surface controllable properties, adjustable pore sizes, and large surface area [25]. In synthetic MOFs, the pore size and channels can be trivial, reaching nanometers and angstrom. At high pressure, these small pores and channels of the MOFs can store CO₂ gas up to 10 to 12 times greater than an empty container [26,27]. It is crucial to choose MOFs with high CO₂ uptake at low pressures to facilitate an effective CO₂ capture process for enclosed localities. Thus, MOFs provide a solid platform for many carbon capture processes. Table 4 below shows the list of abbreviations and acronyms used in this article.

Table 4. List of the abbreviations and acronyms used in this review article.

Abbreviation	Name
MOF	Metal-organic frameworks
HUMs	Hybrid ultra-microporous materials
CCS	Carbon capture and storage
HKUST	Hong Kong university of science and technology
ZIF	Zeolitic imidazolate framework
MIL	Materials of institut lavoisier
TEPA	Tetraethylenepentamine
PIM	Polymer of intrinsic microporosity
TFC	Thin film composite
PDMS	Polydimethylsiloxane
PEBA	Polyether-block-amide
KAUST	King Abdullah university of science and technology
MMM	Mixed-matrix membranes
NPs	Nanoparticles
CNFs	Chitosan nanofibers
GO	Graphene oxide
PSF	Polysulfone
MUF	Massey university framework
PDA	Polydopamine

Table 4. Cont.

Abbreviation	Name
DABCO	Diazabicyclo octane
HOMO	Highest occupied molecular orbital
LUMO	Lowest unoccupied molecular orbital
PL	Photoluminescence
SHE	Standard hydrogen electrode
PIC	Porous interconnected carbon
FE	Faradaic efficiency
ECR	Electrochemical reduction
TMOS	Tetramethyl orthosilicate
CO ₂	Carbon dioxide
N ₂	Nitrogen
CH ₄	Methane
H ₂	Hydrogen
CO	Carbon monoxide
CH ₃ OH	methanol
HCOOH	Formic acid
C ₂ H ₄	Ethylene
HCHO	Formaldehyde
HCOO ⁻	Formate

3. Carbon Dioxide (CO₂) Capture Using Metal-Organic Frameworks

Carbon dioxide capture and storage are now being vigorously investigated to simultaneously combat global climate change while producing more sustainable synthetic fuels to use for several purposes [28–33]. The key approaches for capturing CO₂ using MOFs for the mitigation of the CO₂ emissions resulting from fuel combustion power plants are pre-combustion capture, post-combustion capture, and oxy-fuel combustion capture. The CO₂ capture selection method is mostly based on its advantages, disadvantages, and CO₂ feed input conditions such as partial pressure and concentration of CO₂ in the flue gas. Table 5 below shows a comparison between oxy-fuel combustion capture, pre-combustion capture, and post-combustion capture based on the advantages and disadvantages of each method.

Wang, et al. [34] mentioned that for newly-built power plants, oxy-fuel combustion could be adopted, whereas, for gasification plants, pre-combustion capture is the most appropriate carbon capture approach [34]. Moreover, post-combustion carbon capture is frequently favored for retrofitting power plants, since direct fuel combustion occurs in the boiler of all coal-fired power generation. Zou and Zhu [35] mentioned that the recognition ability of a CO₂ porous adsorbent is usually evaluated by two main key factors: the adsorption capacity of CO₂ and the selectivity of the material. The authors also mentioned that the ideal MOF materials with the high capturing ability of CO₂ are expected to exhibit both high adsorption and high uptake for CO₂ gas over other gases, like CH₄ and N₂ [35]. The effective CO₂ capture ability of MOF materials is owing to their distinguishable chemical and structural features. These unique features include pore size, unsaturated or open metal sites, function control, polar functional groups into the pore channels, and alkylamine incorporation. Kang, et al. [36] stated that the gas separation process is one of the most challenging and critical steps for the industrial processes, and MOFs are potential candidates for this separation application [36]. Table 6 below shows a summary of MOF-based materials for CO₂ capture.

Table 5. Advantages and disadvantages of oxy-fuel combustion capture, pre-combustion capture, and post-combustion capture.

Oxy-Combustion Carbon Capture	Pre-Combustion Carbon Capture	Post-Combustion Carbon Capture
Advantages		
Produce high efficiency steam cycles	Frequently used in the industrial processes	Applicable for existing and new coal-fired power plants
Low level of Pollutants emissions at low cost	Lower energy requirements compared to other CO ₂ capture methods	Extensive studies are made to improve the sorbents and the capture equipment
Cost effective compared to other CO ₂ capture methods. A low cost is required to capture more than 98% of CO ₂	Syngas can be used as a fuel for turbine cycle	Future developments of pulverized coal systems will increase the plant efficiency and reduce CO ₂ emissions
Easy to retrofit into an existing power plant, and does not require an on-site chemical operation	Requires less amount of water compared to post-combustion capture	Most commonly used technology in CO ₂ capture methods
Disadvantages		
High Energy penalty	Significant loss of energy compared to post-combustion capture.	Low CO ₂ partial pressure at ambient pressure
High overall cost	High equipment cost	The amine technologies used results in an almost 30% loss of the net power output and an efficiency reduction of 11%
Technology needs to be proved for large scale operations.	Requires extensive supporting systems	The steam extraction decreases the flow to low-pressure turbine; affecting the efficiency and reducing capability
High risk of CO ₂ leakage	Mainly applicable to new plants	High performance, circulation volume, and water requirements are needed for high capture levels

Table 6. Summary of MOF-based materials CO₂ capture.

MOF	CO ₂ Uptake	T (°C)	P	Ref.
Zn(adc) (4,40-bpe) _{0.5}	130 mmol g ⁻¹	-78.15	1p/p	[37]
(MIL-53)	7.5 mmol g ⁻¹	30.85	20 bar	[38]
Cu(fam) (4,40-bpe) _{0.5}	100 mL g ⁻¹	-78.15	760 torr	[39]
Ni ₂ (cyclam) ₂ (mtb)	57 mL g ⁻¹	-78.15	1 atm	[40]
MIL-53 M = Al, Cr	10 mmol g ⁻¹	30.85	30 bar	[41]
(PCN-5)	210 mg g ⁻¹	-78.15	760 torr	[42]
Cu(dhbc) ₂ (4,40-bpy)	70 mL g ⁻¹	24.85	0.4–8 atm	[43]
Cu(bdc) (4,40-bpy) _{0.5}	70 mL g ⁻¹	24.85	0.1–0.2 MPa	[43]
(ZIF-20)	70 mL g ⁻¹	0	760 torr	[44]
[Ni(bpe) ₂ (N(CN) ₂)] (N(CN) ₂)	35 mL g ⁻¹	-78.15	1p/p	[45]
Zn ₂ (tcom) (4,40-bpy)	5 wt%	24.85	1 bar	[46]
Cu(pyrdc)(bpp)	Differed adsorption capacity	-78.15	Different pressure	[47]
Ni ₃ (BTC) ₂	3.0 mmol g ⁻¹	40	1 bar	[48]
SNU-110	6.0 mmol g ⁻¹	78	1 bar	[49]
1D-MOF	4.0 mmol g ⁻¹	78	1 bar	[50]
2D-MOF	2.9 mmol g ⁻¹	0	1 bar	[51]
A core-shell MOF	41 mmol g ⁻¹	0	1 bar	[52]
NJU-Bai12	23.8 mmol g ⁻¹	0	20 bar	[53]
PCN-124	9.1 mmol g ⁻¹	0	1 bar	[54]
MOF-5/graphite oxide	1.1 mmol g ⁻¹	25	4 bar	[55]
HCM-Cu ₃ (BTC) ₂ -3	2.8 mmol g ⁻¹	25	1 bar	[56]
Zn doped Ni-ZIF-8	4.3 mmol g ⁻¹	0	1 bar	[57]
Zn(II)-based MOFs	9.2 mmol g ⁻¹	25	1 bar	[58]
MOF with PEI	4.2 mmol g ⁻¹	78	0.15 bar	[59]
MIL-53 with BNH _x	4.5 mmol g ⁻¹	0	1 bar	[50]
Mg-MOF-74	8.0 mmol g ⁻¹	23	1 bar	[60]
UMCM-1-NH ₂ -MA	19.8 mmol g ⁻¹	25	18 bar	[61]

Table 6 represents a summary of MOF based materials for CO₂ capture and it is clearly seen that as the temperature increases, the adsorption capacity of CO₂ decreases. Chen, Jin and Chen [62] mentioned in their study that the adsorption capacity and saturated adsorption capacity decreases

with the increase in adsorption temperature. They also added that an exponential function is the best function that describes the relationship between saturated adsorption capacity and temperature. Hence, to obtain a high CO₂ adsorption capacity, the adsorption temperature should be low enough.

3.1. Oxy-Fuel Combustion CO₂ Capture

Oxy-fuel combustion is the process at which hydrocarbon fuel is combusted in a nearly pure oxygen environment, as opposed to air. For controlling the temperature, oxygen is diluted in a portion of the flue gas rather than dilution in nitrogen. In a coal-fired power plant, the oxy-fuel combustion aims to produce flue gas that is enriched with CO₂ and water vapor. This allows the separation or the capture of CO₂ from the flue gas by using low-temperature desulfurization and dehydration processes [63]. Figure 3 below shows a block flow diagram of an oxy-combustion carbon capture system.

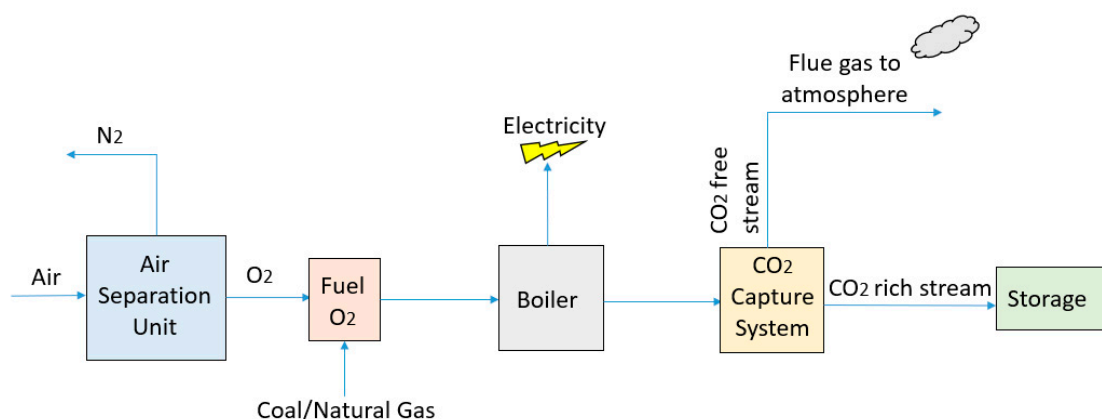


Figure 3. Block flow diagram of an oxy-fuel combustion carbon capture system.

Sumida, et al. [64] stated that oxy-fuel combustion refers to the combustion process in a nearly pure O₂ environment of pulverized coal or other carbonaceous fuel. The significant merit of the oxy-fuel combustion process is based on the fact that the flue gas is almost entirely CO₂. This eases the capture step, and also most of the existing power plants can be easily retrofitted with an oxy-fuel combustion system. Even though there are no full-scale plants that currently adopt oxy-fuel combustion, theoretical studies in combination with pilot-scale and laboratory studies have mentioned some operational issues and important design parameters that aid in studying the oxy-fuel combustion process [64]. The current carbon capture technologies include membranes and MOF-based adsorbents. Hu, et al. [65] mentioned that MOF, activated carbon, and Zeolite adsorbents are all physisorption-based and can be applied to oxyfuel, pre-combustion, post-combustion, and CO₂ capture. The authors also mentioned that as a result of the weak interactions with CO₂, activated carbon, and zeolite adsorbents are unlikely to be used for direct air capture.

On the other hand, MOFs can be tuned to undertake a strong interaction with CO₂ making it suitable for direct air capture processes [65]. The nitrogen-free combustion atmosphere of the oxy-fuel combustion entails a flue gas with a high concentration of CO₂ and water vapors for easier separation. The capture of CO₂ is not required in oxy-fuel combustion since purification can be easily achieved by water vapors condensation. The MOFs' selectivity for other molecules is based on the polarizabilities, diversity of the competing molecules, and the differences between the quadruple moments. Consequently, MOFs have a poor selectivity for O₂/N₂ as a result of the similarity in their molecular nature. Thus, the application of MOFs in the oxy-fuel combustion process is restricted in the carbon capture processes [66].

3.2. Pre-Combustion CO₂ Capture

Pre-combustion carbon capture technology involves capturing the carbon from the fuel before completing the combustion process [67]. A pre-treatment stage is conducted for the fuel, such as natural gas steam reforming, biomass, and coal gasification, before the actual combustion stage [68,69]. Syngas, which is a mixture of CO and H₂, is produced in this pretreatment stage. By using the water gas shift (WGS) reaction, CO in the syngas is then reacted with steam to produce additional CO₂ and H₂ [63]. The separation of H₂ and CO₂ can then be achieved by various technologies. The pre-combustion technology has the merit of lower energy requirements; however, the efficiency and the temperature associated with the H₂-rich gas turbine fuel is considered a big problem. Figure 4 below illustrates a block flow diagram of a pre-combustion carbon capture system.

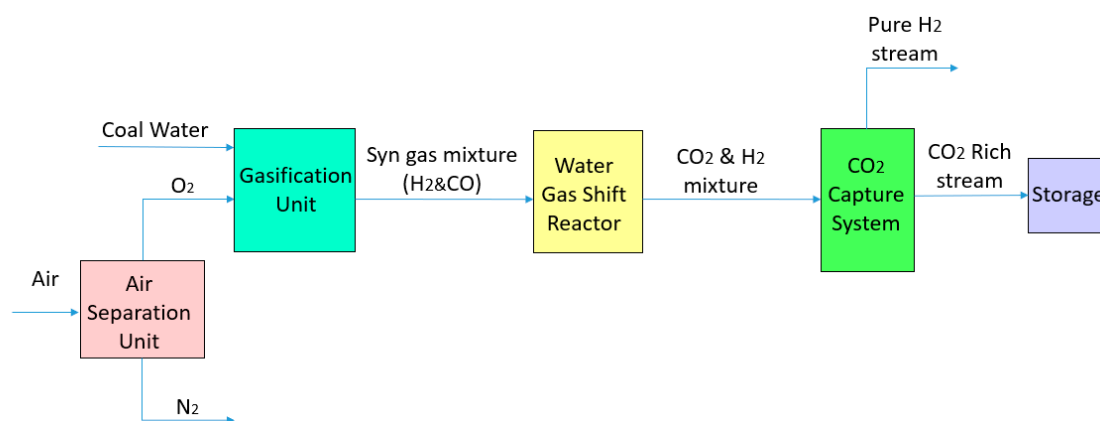


Figure 4. Block flow diagram of pre-combustion carbon capture system.

Lea-Langton and Andrews [70] mentioned that the pre-combustion technology offers a lower-cost CCS since the combined-cycle gas turbine is the base power generator, which has an approximately 62% thermal efficiency in the latest technology plants compared to approximately 50% efficiency in the latest steam-cycle technology [70]. The addition of the MOFs to the pre-combustion processes aids in enhancing the separation of CO₂ from the CO₂/H₂ mixture. Zhang, et al. [71] mentioned that MOFs are better than zeolites as adsorbents for the pre-combustion CO₂/H₂ separation because MOFs possess higher porosities and result in vast uptakes of CO₂ at moderately high pressures [71]. Chung, et al. [72] discovered new MOFs adsorbent material that has a high CO₂ working capacity, which might help in the reduction of CO₂ emissions from the newly commissioned power plants that use the pre-combustion carbon capture technique. The authors have reported the in-silico discovery of high-performance adsorbents for the CO₂ pre-combustion capture. A genetic algorithm was used by the authors to efficiently search for a large database of top candidates of MOFs. The MOFs with the highest performance that were identified from the in-silico search were then synthesized and activated. These MOFs in the study have shown a high CO₂/H₂ selectivity and a CO₂ working capacity. The authors' also mentioned that one of the MOFs that they synthesized had shown the highest CO₂ working capacity compared to all the MOFs reported in the literature under the same operating conditions [72]. Nandi, et al. [73] synthesized MOFs with high CO₂/H₂ selectivity that are suitable for the pre-combustion capture. The authors reported an ultra-microporous (3.5 and 4.8 Å pores) Ni-(4-pyridylcarboxylate) with a working capacity of (3.95 mmol/g), which makes it applicable for hydrogen purification under normal CO₂ pre-combustion capture conditions. The MOFs reported in this study exhibited facile adsorption-desorption CO₂ cycling and have a CO₂ self-diffusivity of approximately 3×10^{-9} m²/s, which is approximately double zeolite 13X [73]. Ding, et al. [74] stated that the usage of MOFs in the CO₂ conversion and capture applications went through three main development stages. First, the CO₂ selectivity and adsorption capacity of MOFs were tuned. Based on that, a large number of strategies were used and investigated for the enhancement of the MOF-CO₂

interactions. The authors also mentioned that with time, many MOFs with strong interactions with CO₂ were developed. Many researchers focused their attention on the applications of pre-combustion carbon capture for CO₂ separation. The authors of the study mentioned that the MOF (Ni-4PyC) is considered as an ideal candidate for pre-combustion of CO₂ capture since, at a very high pressure reaching 35 bar it adsorbed almost no H₂ [74]. Herm, et al. [75] studied some selected MOFs with high structural flexibility, high surface area, or with open metal cation sites, for the utility in CO₂ separation from H₂ using pressure swing adsorption. The authors measured the single-component H₂ and CO₂ adsorption isotherms at a temperature of 313 K and pressures reaching 40 bar. For the pre-combustion CO₂ capture and H₂ purification, ideal adsorbed solution theory was employed by the authors in order to have a realistic estimation of the isotherms for the 80:20 and 60:40 H₂/CO₂ gas mixtures. The results of the authors' study have shown that the MOFs with high concentrations of the exposed metal cation sites, Cu-BTTRI and Mg₂ (dobdc), had significant improvements over the traditional commonly used adsorbents. Thus, those MOFs have promising applications in the CO₂/H₂ separations [75]. Asgari and Queen [76] stated that by considering the limited ability to tune the pore shape, pore size, and surface functionality of the zeolites and activated carbons, only fractional improvements in their separation efficiency can be achieved. On the other hand, the MOFs offer a record-breaking CO₂ adsorption capacity in the pre-combustion CO₂ capture pressure regime. In the meantime, NU-11 has the highest pressure CO₂ adsorption with an absolute uptake of 856 cm³ per gram of MOF at 25 °C and 30 bar. In addition, as mentioned by the authors, the MOFs facile structural tunability can allow significant improvements in the CO₂ binding strength and hence increases the CO₂ selectivity over H₂. Also, the MOFs' surpassing internal surface area is considered a very important factor for high-pressure separations improvements [76]. Sumida, Rogow, Mason, McDonald, Bloch, Herm, Bae and Long [64] mentioned that MOF-based membranes are a promising strategy for pre-combustion CO₂ capture. This is mainly because the pre-combustion gas mixture high pressure is an outstanding driving force for the membrane separation of H₂ and CO₂ [64].

3.3. Post-Combustion CO₂ Capture

The post-combustion carbon capture (PCC) technology is from the most commonly used technologies in the carbon capture field, but there are certain drawbacks and limitations that govern its usage [77–81]. Zamarripa, Eslick, Matuszewski and Miller [79] mentioned that PCC is an expensive energy-intensive process that is subjected to a considerable number of researches using various types of technologies, including sorbents, solvents, and membranes [79]. In the post-combustion carbon capture technology, the carbon-based fuel first undergoes combustion before the separation of the CO₂ from the flue gas is carried out [80]. A pre-treatment of the flue gas has to be conducted for the removal of all the corrosive substances and impurities. Since the flue gas temperature from the combustion units is more likely to be high, ranging from 120 °C to 180 °C, energy-intensive cooling systems are required before pretreatment [82]. Also, because of the high flue gas volume and low CO₂ partial pressure, large size equipment is needed. Both aspects increase the capture cost considerably. Figure 5 below shows a block flow diagram of a post-combustion carbon capture system.

Hu, et al. [83] stated that the post-combustion capture of CO₂ from the flue gas of a coal-fired power plants is a very important and critical approach because the CO₂ emitted from fossil fuel combustion contributed to approximately 60% of total CO₂ worldwide emission in 2004 [2]. Figueroa, et al. [84] mentioned that the flue gas emitted from post-combustion consists of approximately 75% N₂ and 15% CO₂, balanced by other impurities and moisture at ambient pressures (1 bar) and temperatures (30 °C) and pressures (1 bar) [84]. Consequently, an economically viable post-combustion CO₂ capture approach should efficiently separate the 15% CO₂ from the 75% N₂ with the lowest cost at ambient conditions without being affected by the moisture [83].

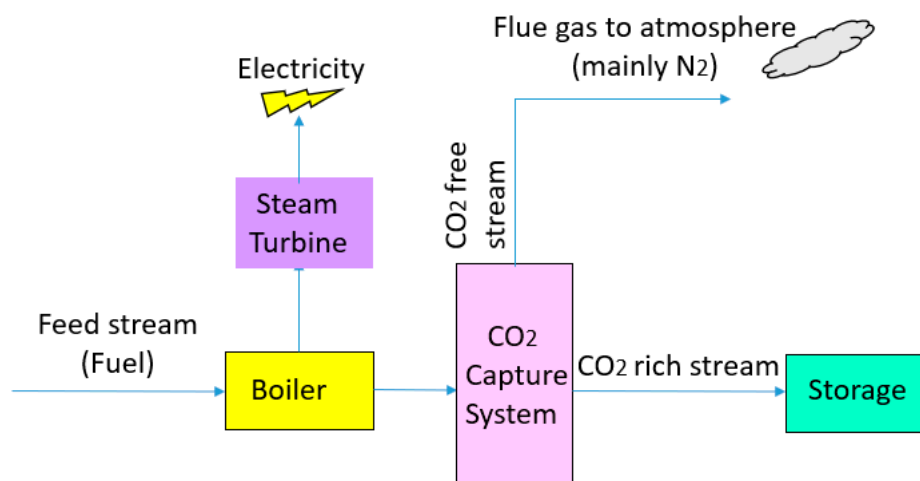


Figure 5. Block flow diagram of post-combustion carbon capture system.

Several studies have been conducted to investigate the efficiency of MOFs in the CO₂ capture under post-combustion conditions. Martínez, et al. [85] investigated three distinct commercial amino-containing MOFs (MIL-53(Al), HKUST-1, and ZIF-8) in the adsorption of CO₂ under post-combustion conditions. The authors' have modified these MOFs by wetness impregnation of tetraethylenepentamine (TEPA) molecules. The results of their study have shown that the amino-impregnated ZIF-8 samples have exhibited higher adsorption capacities by combining the chemical and physical adsorption of CO₂ compared to the TEPA-impregnated microporous framework. Under CO₂ post-combustion capture conditions, the TEPA-impregnated ZIF-8 samples went through a significant increase in the CO₂ uptake reaching 104 mg CO₂/gads, as a result of the moisture present, which governs the CO₂ capture efficiency increase of amino groups [85]. Pai, et al. [86] studied five distinct diamine-appended MOFs that exhibit an S-shaped CO₂ isotherm using a vacuum swing adsorption process in the post-combustion CO₂ capture from dry flue gas. The authors' algorithm to maximize the CO₂ recovery and purity has shown a linkage between the evacuation pressure, feed temperature, and the performance of the process. The MOFs that have achieved a target CO₂ recovery $\geq 90\%$ and purity $\geq 95\%$, namely, mmen-Mg₂ (dobpdc), and mmen-Mn₂ (dobpdc), were optimized by the authors to increase productivity and reduce parasitic energy. The authors also mentioned that the low affinity of N₂ and the distinct shape of the CO₂ isotherm were the main reasons for the lower energy consumption [86].

Hedin, et al. [87] stated that MOFs had been intensively studied as an efficient class of adsorbents for CO₂ capture. Several studies mentioned by the authors have shown that certain members of this class of solid adsorbents can adsorb large quantities of CO₂ while having a higher selectivity of CO₂ over N₂ for the post-combustion capture of CO₂ from flue gas [87]. Furthermore, Samanta, et al. [88] stated that MOFs as a sorbent for the post-combustion capture of CO₂ are expected to have a remarkable and significant adsorption capacity; however, they require substantial, intensive research efforts to be applicable under flue gas conditions. Also, they mentioned that the CO₂/N₂ selectivity further limits the usage of these sorbents for CO₂ adsorption [88]. Maurya and Singh [89] comparatively studied some water-stable microporous adsorbents for post-combustion CO₂ capture. They investigated three metal-organic frameworks (MOFs), a single-wall carbon nanotube (SWCNT) and two covalent organic frameworks (COFs), and a single-wall carbon nanotube (SWCNT) under equal flue gas conditions. The results of the simulation made by the authors depicted that the pure component CO₂ adsorption capacity followed this descending order SWCNT > InOF-1 > COF-300 > UiO-66 > COF-108 > ZIF-8 under post-combustion conditions [89]. Babarao and Jiang [90] reported a computational study for the characterization of the cation and the capture of CO₂ in the Li⁺-exchanged metal-organic frameworks (Li⁺-MOFs). The authors' have adopted a density functional theory for the cation locations

optimization and the evaluation of the atomic charges, and the molecular simulation used to investigate the separation of CO₂/H₂ and CO₂/N₂ gas mixtures for the pre-combustion and post-combustion CO₂ capture. The results of the authors' study show that at ambient conditions, the selectivity is around 60 for CO₂/N₂ mixture and 550 for CO₂/H₂ mixture, higher than the selectivities in other nano-porous adsorbents and the non-ionic MOFs. They also mentioned that the charge of the cations and framework have a remarkable impact on the selectivity, that was found to decrease by a magnitude of 1 order by switching off the charges. Also, the Li⁺-MOF cations' hydration leads to a reduction in the free volume, leading to a lower adsorption extent [90]. Further studies have focused their research on the rule of photoresponsive MOFs in the CO₂ capture under post-combustion conditions. Park, et al. [91] proposed a new photoresponsive MOF, namely Mg-IRMOF-74-III structure with azopyridine molecules bonded to its unsaturated metal sites for CO₂ capture. The authors' computational simulations showed that the photochemical MOF had induced the trans-to-cis transition of the material leading to a remarkable alteration in the capacity of CO₂. Their work aimed to provide a blueprint for the computational design of the new photoresponsive MOF before the actual experimental synthesis [91]. Wang, et al. [92] also mentioned that MOFs, with their distinguishable characteristics and their fine-tunable structures, are exceptional porous solid materials that can provide many powerful and efficient platforms for the exploration of high-performance adsorbents for the CO₂ post-combustion capture [92].

Marti [93] mentioned that the post-combustion CO₂ capture technology is currently the most utilized method for power production. The CCS targets for the post-combustion CO₂ capture are to achieve 90% CO₂ capture with less than 20% increase in the electricity cost. This financially translates to a CO₂ separation and compression cost of \$30–50 per ton of CO₂ [93]. Moreover, a very remarkable study has synthesized MOFs with no N₂ adsorption. In this study, Hu, et al. [94] post-synthetically tethered distinct alkylamine molecules to the unsaturated Cr (III) centers in the MOF MIL-101 for post-combustion CO₂ capture. The resulting MOFs of their study showed almost no N₂ adsorption with a remarkably increased CO₂ capture as a result of the interaction between CO₂ molecules and amine groups under ambient conditions. The authors stated that MIL-101-diethylenetriamine extraordinary CO₂ uptake, exceptional stability, very high CO₂/N₂ selectivity, and the mild regeneration energy, makes it very promising for CO₂/N₂ separation and post-combustion CO₂ capture [94].

3.4. MOFs as Filler in Mixed-Matrix Membranes for CO₂ Separation

Membrane separation is one of the most efficient and commonly used techniques in the CCS field. However, it is governed by certain limitations, including selectivity, permeability, pore size, fouling, and high cost of the membranes [95,96]. Most of the time, selectivity and permeability of the membranes are the main drawbacks to the efficiency of the membranes. Certain porous materials like MOFs, zeolites [97–99], and activated carbons are incorporated in the membranes to increase its CO₂ separation efficiency. Figure 6 below describes how a MOF-based mixed matrix membrane (MMM) is used for CO₂ capture. Figure 6 shows that the feed gas stream containing CO₂ and CH₄ moves across a MOF-based mixed matrix membrane surface that has a selective permeability to the CO₂ gas over CH₄ gas. The CO₂ gas molecules diffuse through the membrane's pores via the solution-diffusion mechanism forming the permeate. Moreover, the CH₄ gas molecules that did not diffuse through the membrane pores form the retentate. The MOF filler enhances the selectivity and permeability of the membrane, allowing more CO₂ molecules to diffuse through the pores of the membrane.

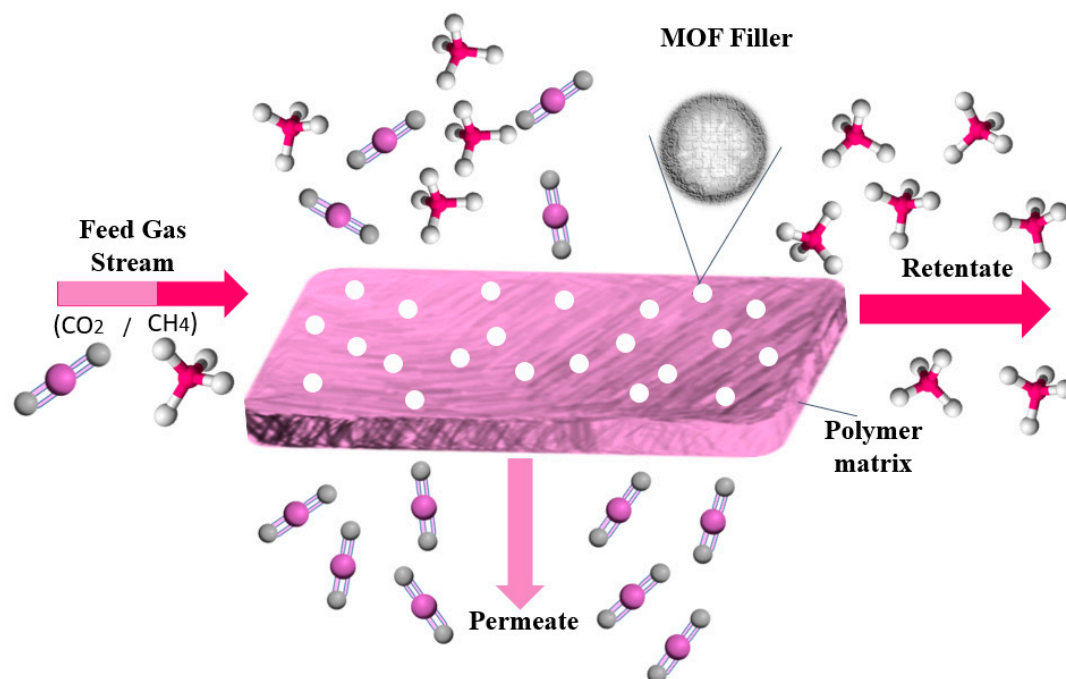


Figure 6. MOF-based mixed matrix membrane (MMM) for CO₂ capture.

With regard to the incorporation of MOFs into the membranes for carbon capture, reference [100] described a thin film composite (TFC) membrane that incorporates MOF nanoparticles and a polymer of intrinsic microporosity (PIM-1) for post-combustion CO₂ capture. The novel TFC membrane design used by the author consists of three layers; the first layer is a CO₂ selective layer synthesized of the mixed matrix PIM-1@MOF. The second layer is an ultra-permeable PDMxS gutter layer that is doped with MOF nanosheets. Moreover, the third layer has a porous polymeric substrate. The results of the study show that the PDMS@MOF gutter layer incorporated with amorphous nanosheets provides a 10,000–11,000 gas permeance units (GPU) permeance of CO₂ permeance. The authors' owes the high CO₂ permeance to the less gas transport resistance compared to the pristine PDMS gutter layers. Furthermore, TFC membrane assembly resulting from a nanosized MOF particles blend (NH₂-UiO-66 and MOF-74-Ni) into PIM-1 improved the permeation of CO₂ 4660–7460 GPU and the selectivity of CO₂/N₂ of 26–33, in comparison to the pristine PIM-1 counterpart with a CO₂ permeance of 4320 GPU and a CO₂/N₂ selectivity of 19. This enhancement in the CO₂ separation after the incorporation of MOFs strongly suggests that MOFs' incorporation into the mixed matrix membranes improves CO₂ separation [100]. Sun, et al. [101] introduced a novel metal-organic framework MOF-801 nanocrystal into a polyether-block-amide (PEBA) polymer in order to synthesize a new mixed-matrix material for the separation of CO₂. The author found that the uniform incorporation of the MOF-801 microporous with preferential adsorption of CO₂ provided selective and fast transport channels for CO₂ over N₂, leading to an increase in both the CO₂/N₂ mixed-gas selectivity and the CO₂ permeance compared with the pure PEBA membrane. Based on the study, the MOF-801/PEBA optimized mixed-matrix composite membrane has shown a highly stabilized separation performance with CO₂/N₂ selectivity of 66 and CO₂ permeance of 22.4 GPU under a mixed-gas permeation test. This shows great potential for CO₂ separation and capture [101]. Chen, et al. [102] studied the CO₂ separation performance of a new type of MMM with a microporous filler of MOF-801 and a polymer matrix of PIM-1. The author's experimental results show that the CO₂-philic MOF-801 filler uniform dispersion provided a channel for a fast, selective CO₂ transport; hence, the MOF-801/PIM-1 MMMs show a greater CO₂ permeability and CO₂/N₂ ideal selectivity over the pure polymer membrane [102]. Majumdar, et al. [103] synthesized Mg-MOF-74 crystals for the preparation of a polymer/Mg-MOF-74 MMMs for the separation of CO₂/CH₄ gas mixture. Activation temperature and time of the Mg-MOF-74 crystals were determined to

enhance the performance of the polymer/Mg-MOF-74 mixed matrix. The authors used a solvent-casting method to incorporate the Mg-MOF-74 crystals into the polyvinyl acetate (PVAc) matrix to form a dense MMM. The results showed that the MMM's mixed gas permeability measurements improved in both the permeability and the selectivity of CO₂ with the increase in the amount of MOF. This suggests a strong CO₂ adsorption selectivity of Mg-MOF-74. Also, the authors' have found that the incorporation of Mg-MOF-74 has reduced the effect of plasticization [103]. Ahmad, et al. [104] investigated the gas separation properties of the MMMs 6FDA-DAM with three types of zirconium-based MOFs nanoparticles (MOF NPs, ca. 40 nm) up to 20 bar. The authors investigated the separation of CO₂/CH₄ at high feed pressure with different CO₂ concentrations in the feed in a temperature range of 35–55 °C. The results of the study show that incorporating Zr-MOFs in the 6FDA-DAM MMMs increased both the CO₂ permeability and the CO₂/CH₄ selectivity of this polymer. This study suggests that 6FDA-DAM Zr-MOF MMMs have great potential in the carbon capture process [104].

The MMMs that are derived from MOF nanocrystals represent a promising alternative for overcoming the trade-off between selectivity and permeability of the pristine polymeric membrane. Chen, et al. [105] incorporated CO₂-philic KAUST-nanocrystals into 6FDA-durene polyimide membrane. This incorporation made by the author has increased the permeability and the selectivity of the MMMs. The developed MMMs in this study has a promising application in the CO₂ capture from natural gas and biogas [105]. Jiamjirangkul, et al. [106] mentioned that for the development of metal-organic frameworks (MOFs) nanofibrous membranes, chitosan nanofibers are a very promising template because of their high surface area with the presence of functional groups for the cationic/anionic binding. In their study, Cu-BTC-integrated chitosan/PVA nanofibrous membrane (Cu-BTC/CNFs) hybrids were synthesized. The CNFs/Cu/BTC-3 synthesized by the authors show an adsorption capacity of CO₂/N₂ over 14 times. Hence, the membrane has a great potential for selective capture and filtration of CO₂ [106]. Lee, et al. [107] prepared a Ni-MOF-74 continuous and defect-free membrane on α -alumina support by using the technique of a layer-by-layer seeding followed by a secondary growth crystallization. The gas permeation properties of the membranes were investigated by the authors for small gases, including CO₂, CH₄, H₂, and N₂. The results of their study showed that the Ni-MOF-74 membrane exhibited a stronger adsorption affinity to CO₂ compared to the other gases, and hence the Ni-MOF-74 membrane CO₂ permeation was dominated by the surface diffusion [107].

There is increasing attention nowadays to MMMs comprised of inorganic fillers scattered in an organic matrix for the separation of gas mixtures due to the membrane enhancement in the material robustness, separation selectivity, and throughput. Anastasiou, et al. [108] developed ZIF-8/graphene oxide (GO) hybrid nanofillers and ZIF-8 MOFs and incorporated them into a polysulfone (PSF) matrix. The authors then tested the membranes for their selectivity and permeation properties for CO₂, CH₄, and N₂. The results highlighted that the PSF+ (ZIF-8/GO) MMMs showed an enhancement in the CO₂ permeability (up to 87% increase) and the selectivity of the CO₂/CH₄ pair (up to 61% increase), compared to the pristine PSF membrane. Also, the selectivity of the PSF+ (ZIF-8/GO) MMM was increased up to 7-fold compared to the PSF + ZIF-8 MMM selectivity. Based on the results, the composite fillers that combine MOFs and the GO functionality have a great potential in boosting and tuning the performance of the polymeric membranes for CO₂ separation from flue gas and natural gas [108]. Inorganic fillers can mainly define the optimal performance of the MMMs. Hence, the development and identification of new inorganic fillers are critical for optimizing the MMMs' performance. MMMs incorporated with MOF fillers are extensively investigated. However, MOF fillers with high performance remain scarce and in high demand. Yin, et al. [109] combined for the first time, an emerging MOF that has an exceptional physicochemical property, namely MUF-15 (Massey University Framework-15), into a MMM with PIM-1. As mentioned by the authors, based on the MUF-15 intrinsic ability to discriminate distinct guest molecules, MUF-15 is considered an impressive filler that delivers the MMMs with excellent CO₂ separation property. Hence, MUF-15 can be proposed as a strategy to further increase the MMM performance [109].

The enhancement of MOF membranes' CO₂ separation performance is attracting the attention of several researchers. Wu, et al. [110] reported a versatile post-modification strategy based on polydopamine (PDA) grafting for the improvement of the MOF membranes' CO₂ separation performance. The PDA was deposited by the authors' on the UiO-66 membrane via a simple and mild process. The results of their study show that the modified PDA/UiO-66 membrane exhibited an enhancement in the CO₂/CH₄ and CO₂/N₂ and selectivities of 28.9 and 51.6, respectively. These selectivity results were 2 to 3 times greater than the MOF membranes that are reported with similar permeance. Moreover, under moist conditions and in the 36 h measurement period, the PDA/UiO-66 membrane prepared in their study exhibited superb long-term stability for the capture of CO₂ [110].

The search for effective carbon-capture materials has allowed the disclosure and institution of nanoporous fluorinated MOFs with a contracted pore system as a CO₂-selective benchmark adsorbent. Chernikova, et al. [111] transplanted/integrated SIFSIX-3-M (M = Cu, Zn, and Ni) MOF adsorbent that encompasses a fluorine moieties with the periodic arrangement in a one-dimensional confined channel, showing a remarkable CO₂ adsorption-based selectivity over H₂ and CH₄ and several other industrially related gas mixtures for carbon capture. The single and mixed-gas permeation tests made by the authors showed that the nanoporous MOF membrane is a highly CO₂-selective membrane that shows a greater CO₂-selectivity over H₂, and CH₄ is limited by the selective adsorption of CO₂ in the SIFSIX-3-M functional and contracted channels [111]. The fabrication and design of novel MMMs with a simultaneously enhanced gas selectivity and permeability are greatly demanded by the industries as membrane technology for large-scale CO₂ capture and storage. Traditional fillers consisting of isotropic bulky particles often limit the interfacial compatibility leading to a great loss in the MMMs' selectivity. Cheng, et al. [112] incorporated chemically stable MOF nanosheets into a highly permeable polymer matrix to synthesize defect-free MMMs. The authors homogeneously dispersed the MOF nanosheets within the polymer matrix, owing to their high aspect ratios that enhances the integration of the polymer-filler. The MMMs prepared by the authors showed a high selective separation performance for CO₂, good antiaging, and anti-pressure abilities, thereby offering a new strategy in the development of advanced membranes for the industrial gas separation applications [112].

The efficient separation of CO₂ from CO₂/CH₄ mixtures with membranes has economic, environmental, and industrial importance. Membrane technologies are currently dominated by polymers due to their processing abilities and low manufacturing costs. However, polymeric membranes suffer from either low gas permeabilities or low selectivities. MOFs are suggested as potential membrane candidates that offer both high selectivity and permeability for CO₂/CH₄ separation. Experimental testing of every single synthesized MOF material as a membrane is not practical due to the availability of thousands of different MOF materials. Altintas and Keskin [113] used a multilevel, high-throughput computational screening methodology to examine the MOF database for membrane-based CO₂/CH₄ separation. MOF membranes offering the best combination of CO₂ permeability (>10⁶ Barrer) and CO₂/CH₄ selectivity (>80) were identified by combining grand canonical Monte Carlo and molecular dynamics simulations. The results revealed that the best MOF membranes are located above the Robeson's upper bound, indicating that they outperform polymeric membranes for CO₂/CH₄ separation. The impact of framework flexibility on the membrane properties of the selected top MOFs was studied by comparing the results of rigid and flexible molecular simulations.

The relationship between the structure of the MOFs and the performance was also investigated to provide atomic-level insights into the design of novel MOFs, which will be useful for CO₂/CH₄ separation processes. Prediction of permeabilities and selectivities of the MMM found the best MOF candidates to incorporate as filler particles into polymers, and it was found that MOF-based MMMs have significantly higher CO₂ permeabilities and moderately higher selectivities than pure polymers [113]. Light-responsive metal-organic frameworks are attracting special attention for their use as a filler in MMMs for CO₂ capture. Prasetya and Ladewig [114] synthesized a new generation-2 light-responsive MOF by using Zn as the metal source and both 1,4-diazabicyclo [2.2.2] octane (DABCO) and 2-phenyldiazanyl terephthalic acid as the ligands. The results showed that Zn-azo-dabco MOF

(Azo-DMOF-1) have exhibited photoresponsive adsorption of CO₂ in both a static and dynamic conditions; this is owed to the abundance of azobenzene functionalities from the ligand. The authors' have also incorporated the MOF as a filler in a mixed matrix membrane with PIM-1 as the polymer matrix and evaluated MMM separation performance for CO₂/N₂ gas mixture. The results of their study showed that azo-DMOF-1 might increase the pristine polymer permeability and selectivity of CO₂. Also, the azo-DMOF-1–PIM-1 composite membranes have a good performance, which has surpassed the 2008 Robeson Upper Bound [114]. Benzaqui, et al. [115] used a microporous Al trimesate-based MOF, namely MIL-96-(Al), as a porous hybrid filler in MMMs for the post-combustion separation of CO₂/N₂. The homogeneous and defect-free MMMs with a high MOF loading (up to 25 wt%) synthesized by the authors have super passed the pure polymer membranes for CO₂/N₂ separation [115]. Maina, et al. [116] reported a new route for the synthesis of hybrid membranes containing inorganic nanoparticles and MOFs with potential applications in several areas, including catalysis, separation, electrochemical, and sensing applications was reported [116]. Zhao, et al. [117] studied at different temperatures, feed compositions and feed pressures, the separation and permeation properties of CO₂/N₂ and CO₂/H₂ mixtures for thin high-quality MOF-5 membranes synthesized by the secondary growth method. The MOF-5 membranes synthesized by the authors under the experimental conditions were studied to offer a selective permeation for CO₂ over N₂ and H₂ in CO₂/N₂ and CO₂/H₂ feed mixture. The results showed that the MOF-5 membranes exhibit high permeance and separation for CO₂. It was mentioned by the authors that the sharp increase in the MOF-5 membranes separation factor with the increase in the feed pressure is an unobserved phenomenon for other inorganic microporous membranes [117]. Hu, et al. [118] mentioned that as a result of the MOFs' functionality, easily tunable porosity, and morphology, they are regarded as an ideal filler for MMMs. Fan, et al. [119] incorporated two isomorphous MOFs Ni₂(l-asp)₂pz and (Ni₂(l-asp)₂bipy with different pore sizes into a poly(ether-block-amide) (Pebax-1657) to synthesize MMMs with gas permeation properties for CO₂, N₂, H₂, and CH₄. The results of their study show that the two series of MMMs showed an enhanced CO₂/H₂ selectivity and CO₂ permeability compared to the pure polymer membrane. Ni₂(l-asp)₂bipy@Pebax-20 have shown the highest CO₂ permeation property in the study of 120.2 barrers with an enhanced CO₂/H₂ selectivity of 32.88 compared to the pure polymer membrane of, respectively, 55.85 barrers and 1.729. This study shows that the synthesized MMMs with MOF fillers are remarkable candidates for the future applications in CO₂ capturing [119].

3.5. MOFs in Photo-Catalytic Conversion of CO₂

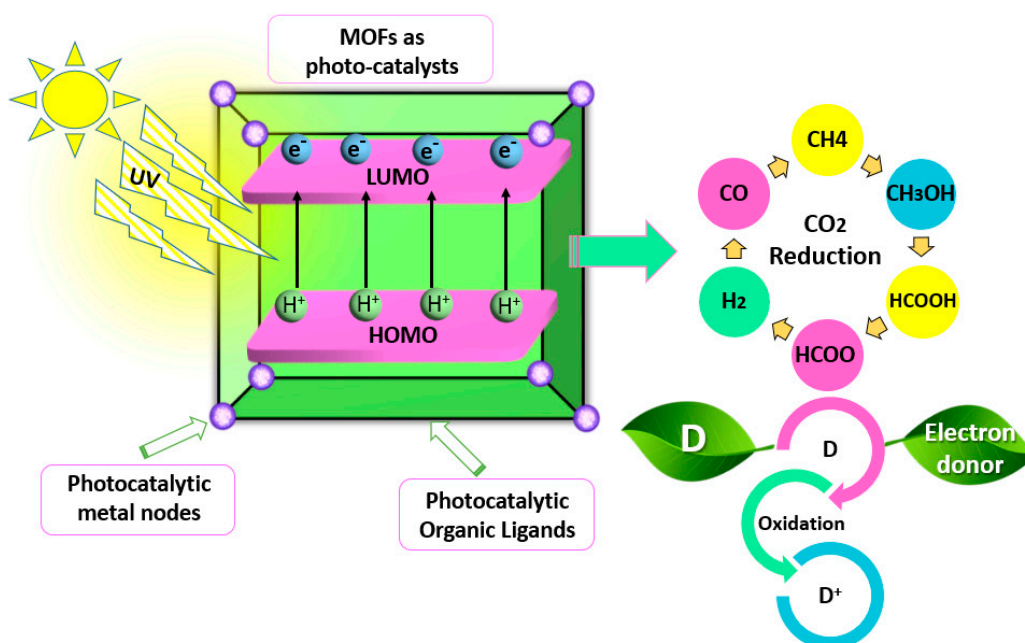
In the road toward a sustainable low-carbon environment, aside from the physical capture and the underground injection and geologic sequestration of the anthropogenic CO₂ emitted from the power plants or industrial processes, catalytic chemical conversion of CO₂ into less harmful valuable chemicals is a very efficient way to undertake the carbon capture process [120–122]. Moreover, CO₂ molecules are very stable as a result of the C=O interactions; multistep reduction via photochemical or electrochemical methods are more imperative than water splitting reactions and have various technical implications. The CO₂ reduction reaction can occur in several distinct pathways that yield a varied range of reduction products, including carbon monoxide (CO) [123–127], methanol (CH₃OH) [128–135], methane (CH₄) [136], ethylene (C₂H₄) [137,138], formic acid (HCOOH) [139], and others [140,141]. Hence, the target product needed is the factor that governs the overall design process for the CO₂ reduction reaction. MOFs have great application as catalysts in the catalytic conversion reactions of CO₂, including conversion of CO₂ to fuels, hydrogenation, cycloaddition, and photo-reduction of CO₂.

The photo-reduction of CO₂ occurs in the presence of ultraviolet (UV) and visible light irradiation. Depending on the reduction potentials, the CO₂ reduction reaction products can include HCHO, CO, CH₃OH, and CH₄. Table 7 below provides the photo-reduction potentials for the CO₂ reduction reaction.

Table 7. [142]: Standard photo-reduction potentials for the CO₂ reduction reaction.

Reduction Potentials of CO ₂	Reduction Potential vs. Normal Hydrogen Electrode (NHE) (V)
$\text{CO}_2 + \text{e}^- \rightarrow \text{CO}_2^-$	-1.9
$\text{CO}_2 + 2\text{H}^+ + 2\text{e}^- \rightarrow \text{CO} + \text{H}_2\text{O}$	-0.53
$\text{CO}_2 + 2\text{H}^+ + 2\text{e}^- \rightarrow \text{HCOOH}$	-0.61
$\text{CO}_2 + 4\text{H}^+ + 4\text{e}^- \rightarrow \text{HCHO} + \text{H}_2\text{O}$	-0.48
$\text{CO}_2 + 2\text{H}^+ + 2\text{e}^- \rightarrow \text{HCOO}^-$	-0.49
$\text{CO}_2 + 6\text{H}^+ + 6\text{e}^- \rightarrow \text{CH}_3\text{OH} + \text{H}_2\text{O}$	-0.38
$2\text{H}^+ + 2\text{e}^- \rightarrow \text{H}_2$	-0.41
$\text{H}_2\text{O} \rightarrow \frac{1}{2} \text{O}_2 + 2\text{H}^+ + 2\text{e}^-$	+0.41
$\text{CO}_2 + 8\text{H}^+ + 8\text{e}^- \rightarrow \text{HCHO} + \text{H}_2\text{O}$	-0.24

The photocatalytic CO₂ reduction process comprises a series of reactions including adsorption of CO₂, charge carrier separation and transportation, electron-hole pair photo-generation, and chemical reactions between the charge carriers and surface species [143–145]. However, certain photo-induced electrons on the surface of the catalyst are specifically utilized for CO₂ reduction. Consequently, catalysts with high redox potential and relatively low bandgap value are favorable. The photo-induced activation of CO₂ on the surface of MOFs includes some main steps. The catalytic material first adsorbs a photon leading to electron-hole pair separation. This separation excites a negative electron (e⁻) from the highest occupied molecular orbital (HOMO) to the lowest unoccupied molecular orbital (LUMO), forming a positive hole (H⁺) on the HOMO [146]. The CO₂ molecules are then absorbed on the MOFs' catalytic center and accept electrons forming different products such as CH₄, CO, and HCOOH. The mechanism of the CO₂ photo-reduction process on MOFs is shown in Figure 7. Nevertheless, not all MOFs exhibit photocatalytic activity, and their electronic properties are identical. This may be determined based on the HOMO and LUMO of MOF materials.

**Figure 7.** CO₂ photo-reduction process mechanism on MOFs.

The construction of MOF-based photo- and electro-catalysts is very promising as a result of their considerable flexible structures and active sites. Reddy, et al. [147] mentioned that MOFs are an emerging new class of functional materials with a highly porous structure, exceptional specific surface areas, and tunable surface chemistry; hence, they hold great potential as photocatalysts [147].

Wang, et al. [148] stated that the photocatalytic reduction of CO₂ for valuable chemicals is an attractive way to create a better overall environment. The authors have proposed two distinct conversion processes. In the first process, CO₂ is split into CO, and in the second process, CO₂ is converted into organic chemicals (like CH₃OH, CH₄, and HCOOH) [148]. It is clear that MOFs have a bright future, prospect, and applications in the field of CO₂ photocatalytic reduction. Table 8 below shows a summary of MOF-based catalysts for photocatalytic CO₂ reduction.

Table 8. Summary of MOF-based catalysts for photocatalytic CO₂ reduction.

Sample ID	Proton Donor	Products and Yield (μ mol/g h)			Light Source	Reference
MOF4	TEA	CO	10.9	–	–	UV [149]
Zn ₂ GeO ₄ /ZIF-8	H ₂ O	CH ₃ OH	0.22	–	–	UV [150]
NH ₂ -MIL-125(Ti)	TEOA	HCOO [−]	16.3	–	–	Visible [151]
Cu ₃ (BTC) ₂ @TiO ₂	H ₂ O	CH ₄ ^a	2.64	–	–	UV [152]
Copper porphyrin MOF ^b	TEOA	CH ₃ OH ^c	262.6	–	–	Visible [153]
Pt-NH ₂ -MIL-125(Ti)	TEOA	HCOO	32.4	–	–	[154]
Au-NH ₂ -MIL-125(Ti)			16.3	–	–	
NH ₂ -UiO-66(Zr)	TEOA	HCOO ^d	3.4	–	–	Visible [155]
NH ₂ -UiO-66(Zr/Ti)			5.8	–	–	
Ui-66-CrCAT	TEOA	HCOOH	1724	–	–	[156]
Ui-66-GaCAT			959	–	–	
Co-ZIF-9	TEOA	CO	12.6	H ₂	2.8	Visible [157]
Co-MOF-74			9.9		1.9	
Mn-MOF-74			0.3		0.5	
Zn-ZIF-8			0.2		0.2	
CPO-27-Mg/TiO ₂	H ₂ O	CO	4.09	CH ₄	2.35	UV [158]
TiO ₂			2.25		1.37	
CPO-27-Mg			0		0	
Co-ZIF-9/TiO ₂	H ₂ O	CO	8.8	H ₂	2.6	UV-Vis [159]
Zn/PMOF	H ₂ O	CH ₄	8.7	–	–	UV-Vis [160]
PCN-22	TEOA	HCOO	52.8	–	–	Visible [161]
2Cu/ZIF-8/N ₂	Na ₂ SO ₃	CH ₃ OH ^e	35.82	–	–	Visible [162]
Ag@Co-ZIF-9	TEOA	CO ^f	28.4	H ₂	22.9	Visible [163]
Ni MOFs	TEOA	CO	12.5	H ₂	0.28	Visible [164]
TiO ₂ /Cu ₂ O/Cu ₃ (BTC) ₂	H ₂ O	CO	210	CH ₄	160	Visible [165]
CdS/UiO-bpy/Co	TEOA	CO	235	–	–	Visible [165]
NH ₂ -rGO (5 wt%)/Al-PMOF	TEOA	HCOO	685.6	–	–	Visible [166]
Zn-MOF nanosheets/[CO ₂ (OH)L](ClO ₄) ₃	TEOA	CO	14.45	H ₂	2.6	Visible [167]

^a Average after 4-h operation. ^b (5,10,15,20-tetrakis(4-carboxyphenyl) porphyrin. ^c Production in (ppm/gcat) after 1-h operation. ^d Production in (mmol/molcat) after 10 h operation. ^e Production in (mmol/L g) after 6-h operation. ^f Production in (mmol after) 0.5-h operation.

By looking at Table 8 above, which summarizes MOF-based catalysts for photocatalytic CO₂ reduction, the highest and lowest yields for CO are produced by CdS/UiO-bpy/Co and TiO₂, yielding 235 and 2.25 μ mol/g h, respectively. In addition, the highest and lowest yields for CH₃OH are produced by TEOA and Zn₂GeO₄/ZIF-8 yielding 262.6, and 0.22 μ mol/g h, respectively. Furthermore, the highest and lowest yield for HCOO is produced by TEOA and NH₂-UiO-66(Zr), yielding 685.6 and 3.4 μ mol/g h, respectively. These results prove that MOFs are successfully capable of photo catalytically, reducing CO₂ into other useful products.

Photocatalytic reduction of CO₂ into highly valuable added chemicals via clean, renewable solar energy sources is a remarkable pathway to address the environmental and energy issues. In recent

days, MOFs have been exploited intensively as catalysts for the photocatalytic reduction of CO₂ owing to their extinguishable CO₂ capture abilities, photochemical and structural properties. Li, et al. [168] studied the recent progress made in the MOF-based photocatalysts for the reduction of CO₂ on the basis of the products reduced, including the CO₂ photocatalytic conversion into CO and other organic chemicals (methanol, formic acid, and methane). The authors' have also mentioned several modification techniques for the relevant improvements in the photocatalytic performance and the structural activity-corresponding relationships. The authors have mainly focused on the CO₂ capture capacity role for the CO₂ photocatalytic reduction performance over the MOF-based materials [168]. Li, et al. [169] constructed a MOF that incorporates unsaturated metal sites and accessible nitrogen-rich groups by using a solvothermal assembly of an acylamide-containing Cu(II) ions and tetracarboxylate ligand. The results showed that the MOFs synthesized had a high CO₂-adsorbing capability, and high porosity exposed Lewis acid metal sites. The inherent structural features of the MOFs synthesized in the study makes them very promising candidates as heterogeneous catalysts for the chemical conversion of CO₂; this was confirmed by their highly efficient CO₂ cycloaddition with the small-sized epoxides in the study.

The high efficiency and remarkable size selectivity on the CO₂ catalytic conversion allows the synthesized MOFs in the study to act as an advanced heterogeneous catalyst for the carbon fixation process [169]. Ding, et al. [170] presented an in-situ-growth strategy and a facile double solvent to integrate CdS NPs with MIL-101(Cr) to synthesize CdS/MIL-101(Cr) composite photocatalyst. The results show that under visible light irradiation, the CdS/MIL-101(Cr) exhibited a remarkable activity enhancement for the conversion of CO₂ to CO [170]. Mu, Zhu, Li, Zhang, Su, Lian, Qi, Deng, Zhang, Wang, Zhu and Peng [144] assembled a composite thin film comprised of 2D/2D MOF/rGO heterostructures by using a Coulomb interaction for the use as a co-catalyst for the photocatalytic reduction of CO₂ for the first time. The study results showed that the best thin-film catalyst with an optimal MOF/rGO ratio exhibited a high evolution rate of CO $3.8 \times 10^4 \mu\text{mol h}^{-1} \text{g}_{\text{film}}^{-1}$ (0.46 min^{-1} in TOF) and an acceptable selectivity of 91.74% [144]. Li and Zhu [171] focused their work on the MOF-based materials active sites that achieve efficient charge separation for conductivity in the electrocatalytic CO₂ reduction and visible-light absorption for photocatalytic CO₂ reduction. The authors showed the distinguishable characteristics of the MOF-based material for catalytic CO₂ reduction, the recent progress and development in the MOF-based material for the CO₂ catalytic reduction, and the challenges and future perspectives for the development of MOF-based materials for CO₂ reduction [171].

One of the most effective techniques in the preparation of the catalysts for the CO₂ photocatalytic reduction into high value-added chemicals is by the use of metalloporphyrin as a light-harvesting mixed ligand to optimize the MOF. This method is valuable because it can improve the dispersibility of the porphyrin, thus inhibiting its potential agglomeration. Wang, et al. [172] incorporated through coordination mode a one-pot synthetic strategy to immobilize chemically Cu (II) tetra (4-carboxylphenyl) porphyrin (CuTCPP) into a UiO-66 MOF structure. Also, in-situ growth of the TiO₂ nanoparticles onto the MOF was actualized with the composite's generation of the CuTCPP@UiO-66/TiO₂ (CTU/TiO₂). The results showed that the catalytic results represented an optimal value of $31.32 \mu\text{mol g}^{-1} \text{h}^{-1}$ CO evolution amount, which was approximately 7 times greater than that of the pure TiO₂ obtained using photo-catalysis under Xe lamp irradiation ($\lambda > 300 \text{ nm}$) Wang, Jin, Duan, She, Huang and Wang [172]. Dong, et al. [173] improved the CO₂ conversion activity of a synthesized MOF by the regulation of the metal species in the MOFs metal-cluster nodes, and the MOF's best photocatalytic activity for CO₂ conversion was obtained. The authors' synthesized a stable MOF, PCN-250-Fe₃ with open metal sites and Fe₂^{III}Fe^{II} metal-cluster nodes, and they further improved the CO₂ reduction activity by tuning the M^{II} metal ions species in the cluster. The results of their study showed that all bi-metallic PCN-250-Fe₂M (M = Mn, Ni, Zn, Co) exhibited higher catalytic activity and selectivity for stable reduction of CO₂ into CO, compared to the mono-metallic PCN-250-Fe₃. Further investigations revealed that introducing a second M^{II} metal ions can enhance the migration of the photogenerated

electrons to the active sites and enhance the CO₂ activation and adsorption by favoring the route of CO₂ reduction and limiting the production of hydrogen as an intermediate [173].

CO₂ conversion into clean energy by using photocatalysts with a porous hollow structure that has a superb activity is of worldwide interest. Chen, et al. [174] prepared a porous hollow spheres ZnO/NiO with sheet-like subunits by calcination of Ni–Zn bimetallic organic frameworks. The prepared ZnO/NiO composites showed an improved photocatalytic activity for the CO₂ recondition and an outstanding photocatalytic CO₂ reduction performance [174]. Ye, Gao, Cao, Chen, Yao, Hou and Sun [167] synthesized and used an ultrathin two-dimensional Zn porphyrin-based metal-organic framework (Zn-MOF nanosheets) in the photoreduction of CO₂ to CO. The two novelty noble-metal-free hybrid photocatalytic systems displayed outstanding selectivity and photocatalytic activity for CO emissions under mild photocatalytic reaction conditions. These studies highlight that the development of noble-metal-free photocatalytic systems and MOF-based materials for photocatalytic applications are promising [167]. Crake, et al. [175] effectively coupled under ultraviolet–visible (UV–vis) light irradiation TiO₂ nanosheets and metal-organic framework (NH₂-UiO-66) using an *in-situ* growth strategy for the formation of bifunctional materials for the combined photocatalytic reduction and capture of CO₂. The results of their study showed that the nanocomposites were durable and dramatically more efficient in the reduction of CO₂ to CO than their single components. Furthermore, the photocatalytic activity was significantly altered by the composition of the nanocomposites with the optimal TiO₂ content doubling the evolution rate of CO compared to the pure TiO₂ [175].

3.6. MOF-Based Materials for Electrochemical and Electrocatalytic Conversion of CO₂

Electrochemical and electrocatalytic reduction of CO₂ into hydrocarbons and value-added chemicals is a remarkable and clean way to mitigate greenhouse gas emissions as a result of our over-dependence on fossil fuels. The electrocatalytic CO₂ reduction reaction consists of two half-reactions that can occur by two to fourteen-electron exchange process. These reactions are shown in Table 9, along with various standard electrode potentials vs. the standard hydrogen electrode (SHE).

Table 9. Standard electrochemical potentials for CO₂ reduction [142].

Reduction Potentials of CO ₂	Standard Electrode Potentials vs. SHE (V)
CO ₂ + 2H ⁺ + 2e ⁻ → CO + H ₂ O	-0.106
2CO ₂ + 2H ⁺ + 2e ⁻ → H ₂ C ₂ O ₄	-0.500
CO ₂ + 2H ⁺ + 2e ⁻ → HCOOH + H ₂ O	-0.250
CO ₂ + 4H ⁺ + 4e ⁻ → CH ₂ O + 2H ₂ O	-0.070
CO ₂ + 4H ⁺ + 4e ⁻ → C + 2H ₂ O	0.210
CO ₂ + 8H ⁺ + 8e ⁻ → CH ₄ + 2H ₂ O	0.169
CO ₂ + 6H ⁺ + 6e ⁻ → CH ₃ OH + H ₂ O	0.016
CO ₂ + 14H ⁺ + 14e ⁻ → C ₂ H ₆ + 4H ₂ O	0.084
CO ₂ + 12H ⁺ + 12e ⁻ → C ₂ H ₄ + 4H ₂ O	0.064

Ma, et al. [176] employed Zn–Ni bimetal MOFs as precursors for the synthesis of Ni–N-doped porous interconnected carbon (NiNPIC) catalysts to enhance CO₂RR electrocatalytic activity and selectivity. The interconnected porous structures and the high surface area of the catalyst have provided a convenient channel for mass diffusion and highly accessible Ni–N sites that lead to a higher electron transfer, less interface resistance, and greater electrolyte/gas transport in the CO₂RR. The results demonstrated that the synthesized catalyst has a high conversion efficiency of CO₂ into CO and excellent electrochemical stability at a moderate over-potential [176]. Table 10 below shows a summary of MOF-based catalysts for electrocatalytic CO₂ reduction.

Table 10. Summary of MOF-based catalysts for electrocatalytic CO₂ reduction.

Sample ID	Product	FE (%)	Potential	Reference
Zn-BTC	CH ₄	80.1 ± 6.6	−2.2 V vs. Ag/AgCl	[177]
M-PMOF	CO	98.7	−0.8 V vs. RHE ¹	[178]
Re-SURMOF	CO	93 ± 5	−1.6 V vs. NHE	[179]
ZIF-8	CO	65.5	−1.8 V vs. SCE	[180]
ZIF-CNT-FA-p	CO	100	−0.86 V vs. RHE	[181]
Al ₂ (OH) ₂ TCPP-Co	CO	76	−0.7 V vs. RHE	[182]
CR-MOF	HCOOH	98	−1.2 V vs. SHE	[183]
Ru(III)-doped HKUST1	CH ₃ OH, C ₂ H ₅ OH	47.2	20 mA cm ^{−2}	[184]
Ag ₂ O/layer ZIF	CO	80.5	−1.2 V vs. RHE	[184]
C-AFC@ZIF-8	CO	93	−0.6 V vs. RHE	[185]
ZIF-8 derived Fe-N-C	CO	91	−0.6 V vs. RHE	[186]

¹ Reversible Hydrogen Electrode.

By looking at Table 10 above, CO₂ is mostly electro-catalytically reduced into CO. Furthermore, ZIF-CNT-FA-p shows the greatest FE (%) with a value of 100 for CO. On the other hand, the lowest FE (%) for CO is given by ZIF-8, with a value of 65.

The Cu-based catalysts exhibit distinguishable superiorities; however, achieving high selectivity for hydrocarbon is still a great challenge. Tan, et al. [187] reported a multifunction-coupled Cu–MOF tailor-made electrocatalyst by using time-resolved controllable restructuring from Cu₂O to Cu₂O@Cu–MOF. The restructured electrocatalyst from their study had a high CO₂ adsorption capacity and electrocatalytic activity. The results showed that their synthesized MOF exhibited high performance towards hydrocarbons, with a hydrocarbon Faradaic efficiency (FE) of 79.4% [187]. Li, et al. [188] reported a remarkable 2D bismuth metal–organic framework (Bi-MOF) that exhibits an accessible permanent porosity for a highly efficient CO₂ electrochemical reduction (ECR) to HCOOH. The results of the author’s study show that the 2D Bi-MOF open-framework structure synthesized shows excellent Faradaic efficiency for the formation of HCOOH over a large potential window, reaching 92.2% at approximately −0.9 V [188].

In sustainable energy research, it is well known that metallic copper acts as an electrocatalyst for the CO₂ reduction to multicarbon products like hydrocarbons and alcohols. However, a great challenge remains in the development of a selective, cost-effective, and stable catalyst/electrode material for this reduction reaction. Rayer, et al. [189] studied the potentials of copper carbonized MOF-derived electrocatalysts as catalytic materials for CO₂ electrochemical reduction. The author used two copper-decorated commercial MOFs, PCN-62, and HKUST-1, pyrolyzed at a variable temperature range (400 to 800 °C), were coated on both copper and metallic nickel supports as inks. The authors’ study shows that the MOF-derived coatings produce electrodes with higher selectivity and current density towards isopropanol compared with the uncoated copper electrodes. Also, the best-performing electrocatalyst in their study exhibits an isopropanol Faradaic efficiency (FE) of over 72% [189]. Zhang, et al. [190] synthesized a novel mixed-metallic MOF [Ag₄Co₂(pyz)PDC₄][Ag₂Co(py₂)PDC₂] and transformed it into an Ag-doped Co₃O₄ catalyst that exhibits excellent electrocatalytic performance for CO₂ reduction in water to syngas (H₂ + CO). The as-prepared Ag/Co₃O₄ material showed a high CO selectivity in a 0.1 M KHCO₃ aqueous solution (CO₂ saturated) with an approximately 55.6% corresponding Faradaic efficiency. The results showed that the presence of Ag can increase the efficiency of CO greatly, hence inhibiting the H₂ production [190]. Cao, et al. [191] used a nitrogen-rich Cu–BTT MOF as a catalyst for the electrochemical reduction of CO₂. The results showed that the high-temperature pyrolysis product of Cu–N–C₁₁₀₀ has the best catalytic activity for production of CO and HCOOH [191]. Sun, et al. [192] synthesized nitrogen-doped mesoporous carbon nanoparticles that have atomically dispersed iron sites (namely mesoNC-Fe) using high-temperature pyrolysis of a Fe that contains ZIF-8 MOF. The hydrolysis of tetramethyl orthosilicate (TMOS) in the MOF framework made by the author prior to pyrolysis has a fundamental role in the maintenance of a high surface area

in the formation phase of the carbon structure, impeding the iron (oxide) nanoparticles' formation. The results showed that the combination of such a distinguishable coordination environment that has a high surface area in the mesoNC-Fe carbon structure makes more accessible active sites during catalysis and promotes CO₂ electro-reduction [192].

Transforming CO₂ into a broad range of chemicals, including methanol, is a high priority field of study owing to the direct link between CO₂ emissions and global warming. There is an environmental and industrial need for substituting non-renewable energy fuels with renewable and sustainable energy sources. Electrochemical reduction acts as a superb approach in the conversion of CO₂ to methanol by the employment of alternative energy sources at which an electrocatalyst plays a fundamental role. Many efforts are being made by several researchers to understand and increase the catalytic efficiency of electrocatalysts. MOFs, composite materials, and metal oxide are employed for CO₂ electrochemical reduction to methanol. However, MOFs catch most of the researchers' attention in CO₂ conversion as a result of their high surface area, simplicity, and exquisite structural features. In recent decades, there have been significant applications of MOFs and their derivatives in CO₂ reduction. Al-Rowaili, et al. [193] focused their work on the electro-reduction of CO₂ to methanol by coalescing MOFs' vantages, and their composite materials. The authors highlighted the challenges in achieving CO₂ electro-reduction with high efficiency and selectivity [193]. Dong, et al. [194] introduced a highly stable 3D porphyrin-based MOF of PCN-222(Fe) into a heterogeneous catalysis by using a simple dip-coating method. Their study shows that their composite catalyst PCN-222(Fe)/C exhibited a high catalytic performance for the electrochemical CO₂ conversion to CO with an overpotential of 494 mV and a maximum of 91% FE_{CO} in a CO₂-saturated aqueous solution of 0.5 M KHCO₃ [194].

Hod, et al. [195] demonstrated that MOF material thin-film electrophoretic deposition is an effective method for immobilizing the required quantity of a catalyst. The authors used in their study for electrocatalytic CO₂ reduction a material that consists of functionalized Fe-porphyrins as catalytically competent, redox-conductive linkers. Their method yielded an electrochemically addressable catalytic site with a highly effective surface coverage. The chemical products of their reduction contain mixtures of CO and H₂. These results show that the MOFs are very promising as catalysts for electrochemical reactions [195]. Wang, et al. [196] synthesized a nitrogen-doped carbon via the pyrolysis of a well-known MOF, namely ZIF-8, for the use as a catalyst in the electrochemical reduction of CO₂, and a subsequent acid treatment was then applied. Their study's resulting electrode exhibited a Faradaic efficiency to CO of approximately 78%, with hydrogen the only byproduct [196].

4. Conclusions and Future Perspective

MOFs' applications in the CO₂ capture, adsorption, membrane separation, catalytic conversion, and electrochemical reduction processes were analyzed thoroughly in this paper. As an emerging new class of crystalline porous materials, MOFs have attracted great attention over recent decades. The high surface area, high porosity, well-defined structures, and spectacular CO₂ adsorption of MOFs are in great demand for CO₂ capture, separation, conversion, and reduction processes.

There are three primary approaches in carbon dioxide capture using MOFs: pre-combustion capture, post-combustion capture, and oxy-fuel combustion capture. The post-combustion CO₂ capture is the most adopted technology in the carbon capture field. However, a large number of aspects should be considered before implementing MOFs in these technologies. These aspects include MOFs' adsorption capacity, thermal stability, selectivity, and life cycle in several operational conditions. Also, for large-scale processes, further details should be considered; an economic analysis must be conducted, the supply chain of the raw materials, including the MOFs, should be analyzed, and environmental impact analysis should be produced. In addition, the thermal stability for the MOFs should be increased for large-scale processes by regenerating the MOFs. This increase in thermal stability will allow the MOFs to be used under high operational conditions. Optimistically, MOFs' properties are continually improving and developing over time, which allows them to serve as the next generation material class for CO₂ capture.

In the membrane separation process of CO₂, MOFs act as a filler in mixed matrix membranes, enhancing the membranes' separation efficiency. However, the membrane separation process is usually hindered by several factors, including the cost, permeability, and selectivity of the membrane. The greatest challenge in the membrane separation with MOFs is the cost. Unfortunately, membranes are usually expensive to develop and maintain; with MOFs' incorporation, they will be even more expensive. Hence, economic MOFs should be chosen as a filler for the mixed matrix membranes for an economically viable process.

In the reduction and conversion processes of CO₂, MOFs acts as a catalyst for the processes. The applications of MOFs as a catalyst for these chemical processes are extensively overviewed in this article. Various parameters should be considered before choosing the MOFs, such as photocatalytic activity, electrical conductivity, and stability. The cost of the MOFs is also the major issue that faces their practical application.

Based on the above studies, MOFs are very promising materials for CO₂ capture, separation, adsorption, and chemical processes. However, their application is mainly suppressed by their high cost. MOFs have a high cost as a result of the costly synthesis of their raw materials. The choice of the MOFs' synthesis approach plays a major role in the economic aspect of the process. The high cost of the MOFs' raw materials is mainly owing to the lack of industrial-scale manufacturing facilities [197]. The MOFs' synthesis process involves sophisticated and time-consuming batch operations with complicated separation techniques and costly organic solvents. Various studies have been conducted to find an efficient approach for reducing the cost of the MOFs. DeSantis, et al. [198] performed a techno-economic analysis to identify the primary factors of MOF adsorbents' high production cost (Mg-MOF-74, Ni-MOF-74, HKAUST-1 and MOF-5) and find approaches for cost reduction. The authors found the cost of the solvent used in the MOFs' synthesis to be the main factor for the high cost. The authors also mentioned that by changing from solvothermal synthesis to liquid assisted grinding and aqueous synthesis it is estimated to decrease the cost by up to 83% [198]. Hence, a detailed economic analysis should be performed before choosing the MOF for any process. With their remarkable properties, MOFs are predicted to be further developed for more economical and efficient applications.

Funding: This research was funded by Qatar Foundation NPRP10-0107-170119.

Acknowledgments: The work was made possible by a grant from the Qatar National Research Fund under the National Priorities Research Program award number NPRP10-0107-170119. Its content is solely the responsibility of the authors and does not necessarily represent the official views of QNRF.

Conflicts of Interest: The authors declare no conflict of interest.

References

1. Smithson, P.A. IPCC, 2001: Climate Change 2001: The Scientific Basis. In *Contribution of Working Group 1 to the Third Assessment Report of the Intergovernmental Panel on Climate Change*; Houghton, J.T., Ding, Y., Griggs, D.J., Noguer, M., van der Linden, P.J., Dai, X., Maskell, K., Johnson, C.A., Eds.; Cambridge University Press: Cambridge, UK; New York, NY, USA, 2001; Volume 22, p. 1144, ISBN 0-521-01495-6. [[CrossRef](#)]
2. Lemke, P.; Ren, J.F.; Alley, R.; Allison, I.; Carrasco, J.; Flato, G.; Fujii, Y.; Kaser, G.; Mote, P.; Thomas, R.; et al. IPCC, 2007. *Climate Change 2007. Synthesis Report. Contribution of Working Groups I, II & III to the Fourth Assessment Report of the Intergovernmental Panel on Climate Change*. Geneva; Cambridge University Press: Cambridge, UK; New York, NY, USA, 2007. [[CrossRef](#)]
3. Rochelle, G.T. Amine scrubbing for CO₂ capture. *Science* **2009**, *325*, 1652–1654. [[CrossRef](#)]
4. Thiruvenkatachari, R.; Su, S.; An, H.; Yu, X.X. Post combustion CO₂ capture by carbon fibre monolithic adsorbents. *Prog. Energy Combust. Sci.* **2009**, *35*, 438–455. [[CrossRef](#)]
5. Omoregbe, O.; Mustapha, A.N.; Steinberger-Wilckens, R.; El-Kharouf, A.; Onyeaka, H. Carbon capture technologies for climate change mitigation: A bibliometric analysis of the scientific discourse during 1998–2018. *Energy Rep.* **2020**, *6*, 1200–1212. [[CrossRef](#)]

6. Ghoufi, A.; Maurin, G. Hybrid Monte Carlo Simulations Combined with a Phase Mixture Model to Predict the Structural Transitions of a Porous Metal–Organic Framework Material upon Adsorption of Guest Molecules. *J. Phys. Chem. C* **2010**, *114*, 6496–6502. [[CrossRef](#)]
7. Younas, M.; Rezakazemi, M.; Daud, M.; Wazir, M.B.; Ahmad, S.; Ullah, N.; Inamuddin; Ramakrishna, S. Recent progress and remaining challenges in post-combustion CO₂ capture using metal-organic frameworks (MOFs). *Prog. Energy Combust. Sci.* **2020**, *80*, 100849. [[CrossRef](#)]
8. Qin, J.-S.; Yuan, S.; Alsalmeh, A.; Zhou, H.-C. Flexible Zirconium MOF as the Crystalline Sponge for Coordinative Alignment of Dicarboxylates. *ACS Appl. Mater. Interfaces* **2017**, *9*, 33408–33412. [[CrossRef](#)] [[PubMed](#)]
9. Li, J.-R.; Kuppler, R.J.; Zhou, H.-C. Selective gas adsorption and separation in metal–organic frameworks. *Chem. Soc. Rev.* **2009**, *38*, 1477–1504. [[CrossRef](#)] [[PubMed](#)]
10. Dybtsev, D.N.; Chun, H.; Yoon, S.H.; Kim, D.; Kim, K. Microporous Manganese Formate: A Simple Metal–Organic Porous Material with High Framework Stability and Highly Selective Gas Sorption Properties. *J. Am. Chem. Soc.* **2004**, *126*, 32–33. [[CrossRef](#)]
11. Loiseau, T.; Lecroq, L.; Volkringer, C.; Marrot, J.; Férey, G.; Haouas, M.; Taulelle, F.; Bourrelly, S.; Llewellyn, P.L.; Latroche, M. MIL-96, a Porous Aluminum Trimesate 3D Structure Constructed from a Hexagonal Network of 18-Membered Rings and μ 3-Oxo-Centered Trinuclear Units. *J. Am. Chem. Soc.* **2006**, *128*, 10223–10230. [[CrossRef](#)]
12. Xue, M.; Ma, S.; Jin, Z.; Schaffino, R.M.; Zhu, G.-S.; Lobkovsky, E.B.; Qiu, S.-L.; Chen, B. Robust Metal–Organic Framework Enforced by Triple-Framework Interpenetration Exhibiting High H₂ Storage Density. *Inorg. Chem.* **2008**, *47*, 6825–6828. [[CrossRef](#)]
13. Zhuang, W.; Yuan, D.; Liu, D.; Zhong, C.; Li, J.-R.; Zhou, H.-C. Robust Metal–Organic Framework with An Octatopic Ligand for Gas Adsorption and Separation: Combined Characterization by Experiments and Molecular Simulation. *Chem. Mater.* **2012**, *24*, 18–25. [[CrossRef](#)]
14. Scholes, C.; Kentish, S.; Stevens, G. Carbon Dioxide Separation through Polymeric Membrane Systems for Flue Gas Applications. *Recent Pat. Chem. Eng.* **2010**, *1*. [[CrossRef](#)]
15. Furukawa, H.; Ko, N.; Go, Y.B.; Aratani, N.; Choi, S.B.; Choi, E.; Yazaydin, A.Ö.; Snurr, R.Q.; O’Keeffe, M.; Kim, J.; et al. Ultrahigh Porosity in Metal–Organic Frameworks. *Science* **2010**, *329*, 424. [[CrossRef](#)]
16. Qasem, N.A.A.; Ben-Mansour, R.; Habib, M.A. An efficient CO₂ adsorptive storage using MOF-5 and MOF-177. *Appl. Energy* **2018**, *210*, 317–326. [[CrossRef](#)]
17. Kayal, S.; Sun, B.; Chakraborty, A. Study of metal-organic framework MIL-101(Cr) for natural gas (methane) storage and compare with other MOFs (metal-organic frameworks). *Energy* **2015**, *91*, 772–781. [[CrossRef](#)]
18. Wei, W.; Xia, Z.; Wei, Q.; Xie, G.; Chen, S.; Qiao, C.; Zhang, G.; Zhou, C. A heterometallic microporous MOF exhibiting high hydrogen uptake. *Microporous Mesoporous Mater.* **2013**, *165*, 20–26. [[CrossRef](#)]
19. Joharian, M.; Morsali, A. Ultrasound-assisted synthesis of two new fluorinated metal-organic frameworks (F-MOFs) with the high surface area to improve the catalytic activity. *J. Solid State Chem.* **2019**, *270*, 135–146. [[CrossRef](#)]
20. Mukherjee, S.; Kumar, A.; Zaworotko, M.J. Metal-organic framework based carbon capture and purification technologies for clean environment. In *Metal-Organic Frameworks (MOFs) for Environmental Applications*; Ghosh, S.K., Ed.; Elsevier: Amsterdam, The Netherlands, 2019; pp. 5–61. [[CrossRef](#)]
21. Ghanbari, T.; Abnisa, F.; Wan Daud, W.M.A. A review on production of metal organic frameworks (MOF) for CO₂ adsorption. *Sci. Total Environ.* **2020**, *707*, 135090. [[CrossRef](#)]
22. Kazemi, S.; Safarifard, V. Carbon dioxide capture in MOFs: The effect of ligand functionalization. *Polyhedron* **2018**, *154*, 236–251. [[CrossRef](#)]
23. Duan, C.; Yu, Y.; Xiao, J.; Li, Y.; Yang, P.; Hu, F.; Xi, H. Recent advancements in metal–organic frameworks for green applications. *Green Energy Environ.* **2020**. [[CrossRef](#)]
24. Simmons, J.M.; Wu, H.; Zhou, W.; Yildirim, T. Carbon capture in metal–organic frameworks—A comparative study. *Energy Environ. Sci.* **2011**, *4*, 2177–2185. [[CrossRef](#)]
25. Li, J.-R.; Ma, Y.; McCarthy, M.C.; Sculley, J.; Yu, J.; Jeong, H.-K.; Balbuena, P.B.; Zhou, H.-C. Carbon dioxide capture-related gas adsorption and separation in metal-organic frameworks. *Coord. Chem. Rev.* **2011**, *255*, 1791–1823. [[CrossRef](#)]
26. Li, H.; Eddaoudi, M.; O’Keeffe, M.; Yaghi, O.M. Design and synthesis of an exceptionally stable and highly porous metal-organic framework. *Nature* **1999**, *402*, 276–279. [[CrossRef](#)]

27. Koppens, F.H.L.; Folk, J.A.; Elzerman, J.M.; Hanson, R.; van Beveren, L.H.W.; Vink, I.T.; Tranitz, H.P.; Wegscheider, W.; Kouwenhoven, L.P.; Vandersypen, L.M.K. Control and Detection of Singlet-Triplet Mixing in a Random Nuclear Field. *Science* **2005**, *309*, 1346. [[CrossRef](#)]
28. Ludig, S.; Haller, M.; Bauer, N. Tackling long-term climate change together: The case of flexible CCS and fluctuating renewable energy. *Energy Procedia* **2011**, *4*, 2580–2587. [[CrossRef](#)]
29. Miyagawa, T.; Matsushashi, R.; Murai, S.; Muraoka, M. Comparative assessment of CCS with other technologies mitigating climate change. *Energy Procedia* **2011**, *4*, 5710–5714. [[CrossRef](#)]
30. Koljonen, T.; Flyktman, M.; Lehtilä, A.; Pahkala, K.; Peltola, E.; Savolainen, I. The role of CCS and renewables in tackling climate change. *Energy Procedia* **2009**, *1*, 4323–4330. [[CrossRef](#)]
31. Freund, P. 1 - Anthropogenic climate change and the role of CO₂ capture and storage (CCS). In *Geological Storage of Carbon Dioxide (CO₂)*; Gluyas, J., Mathias, S., Eds.; Woodhead Publishing: Cambridge, UK, 2013; pp. 3–25. [[CrossRef](#)]
32. Hanaoka, T.; Masui, T. Exploring the 2 °C Target Scenarios by Considering Climate Benefits and Health Benefits—Role of Biomass and CCS. *Energy Procedia* **2017**, *114*, 2618–2630. [[CrossRef](#)]
33. Gibbins, J.; Chalmers, H. Is all CCS equal? Classifying CCS applications by their potential climate benefit. *Energy Procedia* **2011**, *4*, 5715–5720. [[CrossRef](#)]
34. Wang, Y.; Zhao, L.; Otto, A.; Robinius, M.; Stolten, D. A Review of Post-combustion CO₂ Capture Technologies from Coal-fired Power Plants. *Energy Procedia* **2017**, *114*, 650–665. [[CrossRef](#)]
35. Zou, X.; Zhu, G. CO₂ Capture with MOF Membranes. In *Microporous Materials for Separation Membranes*; John Wiley & Sons: Hoboken, NJ, USA, 2019; pp. 323–359. [[CrossRef](#)]
36. Kang, Z.; Fan, L.; Sun, D. Recent advances and challenges of metal–organic framework membranes for gas separation. *J. Mater. Chem. A* **2017**, *5*, 10073–10091. [[CrossRef](#)]
37. Chen, B.; Ma, S.; Hurtado, E.J.; Lobkovsky, E.B.; Zhou, H.-C. A Triply Interpenetrated Microporous Metal–Organic Framework for Selective Sorption of Gas Molecules. *Inorg. Chem.* **2007**, *46*, 8490–8492. [[CrossRef](#)]
38. Llewellyn, P.L.; Bourrelly, S.; Serre, C.; Filinchuk, Y.; Férey, G. How hydration drastically improves adsorption selectivity for CO(2) over CH(4) in the flexible chromium terephthalate MIL-53. *Angew. Chem. Int. Ed. Engl.* **2006**, *45*, 7751–7754. [[CrossRef](#)]
39. Chen, B.; Ma, S.; Zapata, F.; Fronczek, F.R.; Lobkovsky, E.B.; Zhou, H.-C. Rationally Designed Micropores within a Metal–Organic Framework for Selective Sorption of Gas Molecules. *Inorg. Chem.* **2007**, *46*, 1233–1236. [[CrossRef](#)]
40. Cheon, Y.E.; Suh, M.P. Multifunctional Fourfold Interpenetrating Diamondoid Network: Gas Separation and Fabrication of Palladium Nanoparticles. *Chem. A Eur. J.* **2008**, *14*, 3961–3967. [[CrossRef](#)]
41. Bourrelly, S.; Llewellyn, P.L.; Serre, C.; Millange, F.; Loiseau, T.; Férey, G. Different Adsorption Behaviors of Methane and Carbon Dioxide in the Isotypic Nanoporous Metal Terephthalates MIL-53 and MIL-47. *J. Am. Chem. Soc.* **2005**, *127*, 13519–13521. [[CrossRef](#)]
42. Ma, S.; Wang, X.-S.; Manis, E.S.; Collier, C.D.; Zhou, H.-C. Metal–Organic Framework Based on a Trinickel Secondary Building Unit Exhibiting Gas-Sorption Hysteresis. *Inorg. Chem.* **2007**, *46*, 3432–3434. [[CrossRef](#)]
43. Kitaura, R.; Seki, K.; Akiyama, G.; Kitagawa, S. Porous Coordination-Polymer Crystals with Gated Channels Specific for Supercritical Gases. *Angew. Chem. Int. Ed.* **2003**, *42*, 428–431. [[CrossRef](#)]
44. Hayashi, H.; Côté, A.P.; Furukawa, H.; O’Keeffe, M.; Yaghi, O.M. Zeolite A imidazolate frameworks. *Nat. Mater.* **2007**, *6*, 501–506. [[CrossRef](#)]
45. Maji, T.K.; Matsuda, R.; Kitagawa, S. A flexible interpenetrating coordination framework with a bimodal porous functionality. *Nat. Mater.* **2007**, *6*, 142–148. [[CrossRef](#)]
46. Thallapally, P.K.; Tian, J.; Radha Kishan, M.; Fernandez, C.A.; Dalgarno, S.J.; McGrail, P.B.; Warren, J.E.; Atwood, J.L. Flexible (breathing) interpenetrated metal-organic frameworks for CO₂ separation applications. *J. Am. Chem. Soc.* **2008**, *130*, 16842–16843. [[CrossRef](#)]
47. Maji, T.K.; Mostafa, G.; Matsuda, R.; Kitagawa, S. Guest-induced asymmetry in a metal-organic porous solid with reversible single-crystal-to-single-crystal structural transformation. *J. Am. Chem. Soc.* **2005**, *127*, 17152–17153. [[CrossRef](#)]
48. Wade, C.R.; Dincă, M. Investigation of the synthesis, activation, and isosteric heats of CO₂ adsorption of the isostructural series of metal–organic frameworks M₃(BTC)₂ (M = Cr, Fe, Ni, Cu, Mo, Ru). *Dalton Trans.* **2012**, *41*, 7931–7938. [[CrossRef](#)]

49. Hong, D.H.; Suh, M.P. Selective CO₂ adsorption in a metal–organic framework constructed from an organic ligand with flexible joints. *Chem. Commun.* **2012**, *48*, 9168–9170. [[CrossRef](#)]
50. Bataille, T.; Bracco, S.; Comotti, A.; Costantino, F.; Guerri, A.; Ienco, A.; Marmottini, F. Solvent dependent synthesis of micro- and nano- crystalline phosphinate based 1D tubular MOF: Structure and CO₂ adsorption selectivity. *CrystEngComm* **2012**, *14*, 7170–7173. [[CrossRef](#)]
51. Yan, Q.; Lin, Y.; Wu, P.; Zhao, L.; Cao, L.; Peng, L.; Kong, C.; Chen, L. Designed Synthesis of Functionalized Two-Dimensional Metal–Organic Frameworks with Preferential CO₂ Capture. *ChemPlusChem* **2013**, *78*, 86–91. [[CrossRef](#)]
52. Li, T.; Sullivan, J.E.; Rosi, N.L. Design and Preparation of a Core–Shell Metal–Organic Framework for Selective CO₂ Capture. *J. Am. Chem. Soc.* **2013**, *135*, 9984–9987. [[CrossRef](#)] [[PubMed](#)]
53. Zheng, B.; Yun, R.; Bai, J.; Lu, Z.; Du, L.; Li, Y. Expanded porous MOF-505 analogue exhibiting large hydrogen storage capacity and selective carbon dioxide adsorption. *Inorg. Chem.* **2013**, *52*, 2823–2829. [[CrossRef](#)] [[PubMed](#)]
54. Park, J.; Li, J.-R.; Chen, Y.-P.; Yu, J.; Yakovenko, A.A.; Wang, Z.U.; Sun, L.-B.; Balbuena, P.B.; Zhou, H.-C. A versatile metal–organic framework for carbon dioxide capture and cooperative catalysis. *Chem. Commun.* **2012**, *48*, 9995–9997. [[CrossRef](#)]
55. Zhao, Y.; Ding, H.; Zhong, Q. Synthesis and characterization of MOF-aminated graphite oxide composites for CO₂ capture. *Appl. Surf. Sci.* **2013**, *284*, 138–144. [[CrossRef](#)]
56. Qian, D.; Lei, C.; Hao, G.-P.; Li, W.-C.; Lu, A.-H. Synthesis of Hierarchical Porous Carbon Monoliths with Incorporated Metal–Organic Frameworks for Enhancing Volumetric Based CO₂ Capture Capability. *ACS Appl. Mater. Interfaces* **2012**, *4*, 6125–6132. [[CrossRef](#)]
57. Yu, J.; Balbuena, P.B. Water Effects on Postcombustion CO₂ Capture in Mg-MOF-74. *J. Phys. Chem. C* **2013**, *117*, 3383–3388. [[CrossRef](#)]
58. Masoomi, M.Y.; Stylianou, K.C.; Morsali, A.; Retailleau, P.; Maspoch, D. Selective CO₂ Capture in Metal–Organic Frameworks with Azine-Functionalized Pores Generated by Mechanochemistry. *Cryst. Growth Des.* **2014**, *14*, 2092–2096. [[CrossRef](#)]
59. Lin, Y.; Yan, Q.; Kong, C.; Chen, L. Polyethyleneimine incorporated metal-organic frameworks adsorbent for highly selective CO₂ capture. *Sci. Rep.* **2013**, *3*, 1859. [[CrossRef](#)]
60. Caskey, S.R.; Wong-Foy, A.G.; Matzger, A.J. Dramatic Tuning of Carbon Dioxide Uptake via Metal Substitution in a Coordination Polymer with Cylindrical Pores. *J. Am. Chem. Soc.* **2008**, *130*, 10870–10871. [[CrossRef](#)] [[PubMed](#)]
61. Xiang, Z.; Peng, X.; Cheng, X.; Li, X.; Cao, D. CNT@Cu₃(BTC)₂ and Metal–Organic Frameworks for Separation of CO₂/CH₄ Mixture. *J. Phys. Chem. C* **2011**, *115*, 19864–19871. [[CrossRef](#)]
62. Chen, S.; Jin, L.; Chen, X. The effect and prediction of temperature on adsorption capability of coal/CH₄. *Procedia Eng.* **2011**, *26*, 126–131. [[CrossRef](#)]
63. Carpenter, S.M.; Long, H.A. 13 - Integration of carbon capture in IGCC systems. In *Integrated Gasification Combined Cycle (IGCC) Technologies*; Wang, T., Stiegel, G., Eds.; Woodhead Publishing: Southorn, UK; Cambridge, UK, 2017; pp. 445–463. [[CrossRef](#)]
64. Sumida, K.; Rogow, D.L.; Mason, J.A.; McDonald, T.M.; Bloch, E.D.; Herm, Z.R.; Bae, T.-H.; Long, J.R. Carbon Dioxide Capture in Metal–Organic Frameworks. *Chem. Rev.* **2012**, *112*, 724–781. [[CrossRef](#)]
65. Hu, Z.; Wang, Y.; Shah, B.B.; Zhao, D. CO₂ Capture in Metal–Organic Framework Adsorbents: An Engineering Perspective. *Adv. Sustain. Syst.* **2019**, *3*, 1800080. [[CrossRef](#)]
66. Günther, C.; Weng, M.; Kather, A. Restrictions and Limitations for the Design of a Steam Generator for a Coal-fired Oxyfuel Power Plant with Circulating Fluidised Bed Combustion. *Energy Procedia* **2013**, *37*, 1312–1321. [[CrossRef](#)]
67. Jansen, D.; Gazzani, M.; Manzolini, G.; Dijk, E.v.; Carbo, M. Pre-combustion CO₂ capture. *Int. J. Greenh. Gas Control* **2015**, *40*, 167–187. [[CrossRef](#)]
68. Looyd, P.J.D. Precombustion technologies to aid carbon capture. In *Greenhouse Gas Control Technologies 7*; Rubin, E.S., Keith, D.W., Gilboy, C.F., Wilson, M., Morris, T., Gale, J., Thambimuthu, K., Eds.; Elsevier Science Ltd.: Oxford, UK, 2005; pp. 1957–1961. [[CrossRef](#)]
69. Zhong, D.-L.; Wang, J.-L.; Lu, Y.-Y.; Li, Z.; Yan, J. Precombustion CO₂ capture using a hybrid process of adsorption and gas hydrate formation. *Energy* **2016**, *102*, 621–629. [[CrossRef](#)]

70. Lea-Langton, A.; Andrews, G. Pre-combustion Technologies. In *Biomass Energy with Carbon Capture and Storage (BECCS): Unlocking Negative Emissions*; Wiley: Hoboken, NJ, USA, 2018; pp. 67–91.
71. Zhang, Z.; Yao, Z.-Z.; Xiang, S.; Chen, B. Perspective of microporous metal–organic frameworks for CO₂ capture and separation. *Energy Environ. Sci.* **2014**, *7*, 2868–2899. [[CrossRef](#)]
72. Chung, Y.G.; Gómez-Gualdrón, D.A.; Li, P.; Leperi, K.T.; Deria, P.; Zhang, H.; Vermeulen, N.A.; Stoddart, J.F.; You, F.; Hupp, J.T.; et al. In silico discovery of metal-organic frameworks for precombustion CO₂ capture using a genetic algorithm. *Sci. Adv.* **2016**, *2*, e1600909. [[CrossRef](#)]
73. Nandi, S.; De Luna, P.; Daff, T.D.; Rother, J.; Liu, M.; Buchanan, W.; Hawari, A.I.; Woo, T.K.; Vaidhyanathan, R. A single-ligand ultra-microporous MOF for precombustion CO₂ capture and hydrogen purification. *Sci. Adv.* **2015**, *1*, e1500421. [[CrossRef](#)]
74. Ding, M.; Flaig, R.W.; Jiang, H.-L.; Yaghi, O.M. Carbon capture and conversion using metal–organic frameworks and MOF-based materials. *Chem. Soc. Rev.* **2019**, *48*, 2783–2828. [[CrossRef](#)] [[PubMed](#)]
75. Herm, Z.R.; Swisher, J.A.; Smit, B.; Krishna, R.; Long, J.R. Metal–Organic Frameworks as Adsorbents for Hydrogen Purification and Precombustion Carbon Dioxide Capture. *J. Am. Chem. Soc.* **2011**, *133*, 5664–5667. [[CrossRef](#)]
76. Asgari, M.; Queen, W. *Carbon Capture in Metal–Organic Frameworks*; Wiley: Hoboken, NJ, USA, 2018; pp. 1–78.
77. Favre, E. Membrane processes and postcombustion carbon dioxide capture: Challenges and prospects. *Chem. Eng. J.* **2011**, *171*, 782–793. [[CrossRef](#)]
78. Tillman, D.A. Chapter Nine—The Development of Postcombustion Control Technology. In *Coal-Fired Electricity and Emissions Control*; Tillman, D.A., Ed.; Butterworth-Heinemann: Oxford, UK, 2018; pp. 237–276. [[CrossRef](#)]
79. Zamarripa, M.A.; Eslick, J.C.; Matuszewski, M.S.; Miller, D.C. Multi-objective Optimization of Membrane-based CO₂ Capture. In *Computer Aided Chemical Engineering*; Eden, M.R., Ierapetritou, M.G., Towler, G.P., Eds.; Elsevier: Amsterdam, The Netherlands, 2018; Volume 44, pp. 1117–1122.
80. Breeze, P. Chapter 7—Carbon Capture and Storage. In *Coal-Fired Generation*; Breeze, P., Ed.; Academic Press: Boston, MA, USA, 2015; pp. 73–86. [[CrossRef](#)]
81. Ghoshal, S.; Zeman, F. Carbon dioxide (CO₂) capture and storage technology in the cement and concrete industry. In *Developments and Innovation in Carbon Dioxide (CO₂) Capture and Storage Technology*; Maroto-Valer, M.M., Ed.; Woodhead Publishing: Cambridge, UK, 2010; Volume 1, pp. 469–491.
82. Spigarelli, B.P.; Kawatra, S.K. Opportunities and challenges in carbon dioxide capture. *J. CO₂ Util.* **2013**, *1*, 69–87. [[CrossRef](#)]
83. Hu, Z.; Khurana, M.; Seah, Y.H.; Zhang, M.; Guo, Z.; Zhao, D. Ionized Zr-MOFs for highly efficient post-combustion CO₂ capture. *Chem. Eng. Sci.* **2015**, *124*, 61–69. [[CrossRef](#)]
84. Figueroa, J.D.; Fout, T.; Plasyński, S.; McIlvried, H.; Srivastava, R.D. Advances in CO₂ capture technology—The U.S. Department of Energy’s Carbon Sequestration Program. *Int. J. Greenh. Gas Control* **2008**, *2*, 9–20. [[CrossRef](#)]
85. Martínez, F.; Sanz, R.; Orcajo, G.; Briones, D.; Yáñez, V. Amino-impregnated MOF materials for CO₂ capture at post-combustion conditions. *Chem. Eng. Sci.* **2016**, *142*, 55–61. [[CrossRef](#)]
86. Pai, K.N.; Baboolal, J.D.; Sharp, D.A.; Rajendran, A. Evaluation of diamine-appended metal-organic frameworks for post-combustion CO₂ capture by vacuum swing adsorption. *Sep. Purif. Technol.* **2019**, *211*, 540–550. [[CrossRef](#)]
87. Hedin, N.; Andersson, L.; Bergström, L.; Yan, J. Adsorbents for the post-combustion capture of CO₂ using rapid temperature swing or vacuum swing adsorption. *Appl. Energy* **2013**, *104*, 418–433. [[CrossRef](#)]
88. Samanta, A.; Zhao, A.; Shimizu, G.K.H.; Sarkar, P.; Gupta, R. Post-Combustion CO₂ Capture Using Solid Sorbents: A Review. *Ind. Eng. Chem. Res.* **2012**, *51*, 1438–1463. [[CrossRef](#)]
89. Maurya, M.; Singh, J.K. Effect of Ionic Liquid Impregnation in Highly Water-Stable Metal–Organic Frameworks, Covalent Organic Frameworks, and Carbon-Based Adsorbents for Post-combustion Flue Gas Treatment. *Energy Fuels* **2019**, *33*, 3421–3428. [[CrossRef](#)]
90. Babarao, R.; Jiang, J.W. Cation Characterization and CO₂ Capture in Li⁺-Exchanged Metal–Organic Frameworks: From First-Principles Modeling to Molecular Simulation. *Ind. Eng. Chem. Res.* **2011**, *50*, 62–68. [[CrossRef](#)]
91. Park, J.; Suh, B.L.; Kim, J. Computational Design of a Photoresponsive Metal–Organic Framework for Post Combustion Carbon Capture. *J. Phys. Chem. C* **2020**, *124*, 13162–13167. [[CrossRef](#)]

92. Wang, Q.; Bai, J.; Lu, Z.; Pan, Y.; You, X. Finely tuning MOFs towards high-performance post-combustion CO₂ capture materials. *Chem. Commun.* **2016**, *52*, 443–452. [[CrossRef](#)]
93. Marti, A. *Metal-Organic Frameworks Materials for Post-Combustion CO₂ Capture*; Wiley: Hoboken, NJ, USA, 2018; pp. 79–111.
94. Hu, Y.; Verdegaal, W.M.; Yu, S.-H.; Jiang, H.-L. Alkylamine-Tethered Stable Metal–Organic Framework for CO₂ Capture from Flue Gas. *ChemSusChem* **2014**, *7*, 734–737. [[CrossRef](#)]
95. Siagian, U.W.R.; Raksajati, A.; Himma, N.F.; Khoiruddin, K.; Wenten, I.G. Membrane-based carbon capture technologies: Membrane gas separation vs. membrane contactor. *J. Nat. Gas Sci. Eng.* **2019**, *67*, 172–195. [[CrossRef](#)]
96. Khalilpour, R.; Mumford, K.; Zhai, H.; Abbas, A.; Stevens, G.; Rubin, E.S. Membrane-based carbon capture from flue gas: A review. *J. Clean. Prod.* **2015**, *103*, 286–300. [[CrossRef](#)]
97. Krishna, R.; van Baten, J.M. In silico screening of zeolite membranes for CO₂ capture. *J. Membr. Sci.* **2010**, *360*, 323–333. [[CrossRef](#)]
98. Chen, Y.; Wang, B.; Zhao, L.; Dutta, P.; Winston Ho, W.S. New Pebax®/zeolite Y composite membranes for CO₂ capture from flue gas. *J. Membr. Sci.* **2015**, *495*, 415–423. [[CrossRef](#)]
99. Zhao, L.; Chen, Y.; Wang, B.; Sun, C.; Chakraborty, S.; Ramasubramanian, K.; Dutta, P.K.; Ho, W.S.W. Multilayer polymer/zeolite Y composite membrane structure for CO₂ capture from flue gas. *J. Membr. Sci.* **2016**, *498*, 1–13. [[CrossRef](#)]
100. Liu, M.; Nothling, M.D.; Webley, P.A.; Jin, J.; Fu, Q.; Qiao, G.G. High-throughput CO₂ capture using PIM-1@MOF based thin film composite membranes. *Chem. Eng. J.* **2020**, *396*, 125328. [[CrossRef](#)]
101. Sun, J.; Li, Q.; Chen, G.; Duan, J.; Liu, G.; Jin, W. MOF-801 incorporated PEBA mixed-matrix composite membranes for CO₂ capture. *Sep. Purif. Technol.* **2019**, *217*, 229–239. [[CrossRef](#)]
102. Chen, W.; Zhang, Z.; Hou, L.; Yang, C.; Shen, H.; Yang, K.; Wang, Z. Metal-organic framework MOF-801/PIM-1 mixed-matrix membranes for enhanced CO₂/N₂ separation performance. *Sep. Purif. Technol.* **2020**, *250*, 117198. [[CrossRef](#)]
103. Majumdar, S.; Tokay, B.; Martin-Gil, V.; Campbell, J.; Castro-Muñoz, R.; Ahmad, M.Z.; Fila, V. Mg-MOF-74/Polyvinyl acetate (PVAc) mixed matrix membranes for CO₂ separation. *Sep. Purif. Technol.* **2020**, *238*, 116411. [[CrossRef](#)]
104. Ahmad, M.Z.; Peters, T.A.; Konnertz, N.M.; Visser, T.; Téllez, C.; Coronas, J.; Fila, V.; de Vos, W.M.; Benes, N.E. High-pressure CO₂/CH₄ separation of Zr-MOFs based mixed matrix membranes. *Sep. Purif. Technol.* **2020**, *230*, 115858. [[CrossRef](#)]
105. Chen, K.; Xu, K.; Xiang, L.; Dong, X.; Han, Y.; Wang, C.; Sun, L.-B.; Pan, Y. Enhanced CO₂/CH₄ separation performance of mixed-matrix membranes through dispersion of sorption-selective MOF nanocrystals. *J. Membr. Sci.* **2018**, *563*, 360–370. [[CrossRef](#)]
106. Jiamjirangkul, P.; Inprasit, T.; Intasanta, V.; Pangon, A. Metal organic framework-integrated chitosan/poly(vinyl alcohol) (PVA) nanofibrous membrane hybrids from green process for selective CO₂ capture and filtration. *Chem. Eng. Sci.* **2020**, *221*, 115650. [[CrossRef](#)]
107. Lee, D.-J.; Li, Q.; Kim, H.; Lee, K. Preparation of Ni-MOF-74 membrane for CO₂ separation by layer-by-layer seeding technique. *Microporous Mesoporous Mater.* **2012**, *163*, 169–177. [[CrossRef](#)]
108. Anastasiou, S.; Bhorina, N.; Pokhrel, J.; Kumar Reddy, K.S.; Srinivasakannan, C.; Wang, K.; Karanikolos, G.N. Metal-organic framework/graphene oxide composite fillers in mixed-matrix membranes for CO₂ separation. *Mater. Chem. Phys.* **2018**, *212*, 513–522. [[CrossRef](#)]
109. Yin, H.; Alkaş, A.; Zhang, Y.; Zhang, Y.; Telfer, S.G. Mixed matrix membranes (MMMs) using an emerging metal-organic framework (MUF-15) for CO₂ separation. *J. Membr. Sci.* **2020**, *609*, 118245. [[CrossRef](#)]
110. Wu, W.; Li, Z.; Chen, Y.; Li, W. Polydopamine-Modified Metal–Organic Framework Membrane with Enhanced Selectivity for Carbon Capture. *Environ. Sci. Technol.* **2019**, *53*, 3764–3772. [[CrossRef](#)] [[PubMed](#)]
111. Chernikova, V.; Shekhah, O.; Belmabkhout, Y.; Eddaoudi, M. Nanoporous Fluorinated Metal–Organic Framework-Based Membranes for CO₂ Capture. *ACS Appl. Nano Mater.* **2020**, *3*, 6432–6439. [[CrossRef](#)]
112. Cheng, Y.; Tavares, S.R.; Doherty, C.M.; Ying, Y.; Sarnello, E.; Maurin, G.; Hill, M.R.; Li, T.; Zhao, D. Enhanced Polymer Crystallinity in Mixed-Matrix Membranes Induced by Metal–Organic Framework Nanosheets for Efficient CO₂ Capture. *ACS Appl. Mater. Interfaces* **2018**, *10*, 43095–43103. [[CrossRef](#)] [[PubMed](#)]

113. Altintas, C.; Keskin, S. Molecular Simulations of MOF Membranes and Performance Predictions of MOF/Polymer Mixed Matrix Membranes for CO₂/CH₄ Separations. *ACS Sustain. Chem. Eng.* **2019**, *7*, 2739–2750. [[CrossRef](#)]
114. Prasetya, N.; Ladewig, B.P. New Azo-DMOF-1 MOF as a Photoresponsive Low-Energy CO₂ Adsorbent and Its Exceptional CO₂/N₂ Separation Performance in Mixed Matrix Membranes. *ACS Appl. Mater. Interfaces* **2018**, *10*, 34291–34301. [[CrossRef](#)]
115. Benzaqui, M.; Pillai, R.S.; Sabetghadam, A.; Benoit, V.; Normand, P.; Marrot, J.; Menguy, N.; Montero, D.; Shepard, W.; Tissot, A.; et al. Revisiting the Aluminum Trimesate-Based MOF (MIL-96): From Structure Determination to the Processing of Mixed Matrix Membranes for CO₂ Capture. *Chem. Mater.* **2017**, *29*, 10326–10338. [[CrossRef](#)]
116. Maina, J.W.; Schütz, J.A.; Grundy, L.; Des Ligneris, E.; Yi, Z.; Kong, L.; Pozo-Gonzalo, C.; Ionescu, M.; Dumée, L.F. Inorganic Nanoparticles/Metal Organic Framework Hybrid Membrane Reactors for Efficient Photocatalytic Conversion of CO₂. *ACS Appl. Mater. Interfaces* **2017**, *9*, 35010–35017. [[CrossRef](#)] [[PubMed](#)]
117. Zhao, Z.; Ma, X.; Kasik, A.; Li, Z.; Lin, Y.S. Gas Separation Properties of Metal Organic Framework (MOF-5) Membranes. *Ind. Eng. Chem. Res.* **2013**, *52*, 1102–1108. [[CrossRef](#)]
118. Hu, Z.; Kang, Z.; Qian, Y.; Peng, Y.; Wang, X.; Chi, C.; Zhao, D. Mixed Matrix Membranes Containing UiO-66(Hf)-(OH)₂ Metal–Organic Framework Nanoparticles for Efficient H₂/CO₂ Separation. *Ind. Eng. Chem. Res.* **2016**, *55*, 7933–7940. [[CrossRef](#)]
119. Fan, L.; Kang, Z.; Shen, Y.; Wang, S.; Zhao, H.; Sun, H.; Hu, X.; Sun, H.; Wang, R.; Sun, D. Mixed Matrix Membranes Based on Metal–Organic Frameworks with Tunable Pore Size for CO₂ Separation. *Cryst. Growth Des.* **2018**, *18*, 4365–4371. [[CrossRef](#)]
120. Takht Ravanchi, M.; Sahebdehfar, S. Catalytic conversions of CO₂ to help mitigate climate change: Recent process developments. *Process Saf. Environ. Prot.* **2021**, *145*, 172–194. [[CrossRef](#)]
121. Dewangan, N.; Hui, W.M.; Jayaprakash, S.; Bawah, A.-R.; Poerjoto, A.J.; Jie, T.; Jangam, A.; Hidajat, K.; Kawi, S. Recent progress on layered double hydroxide (LDH) derived metal-based catalysts for CO₂ conversion to valuable chemicals. *Catal. Today* **2020**. [[CrossRef](#)]
122. Galadima, A.; Muraza, O. Catalytic thermal conversion of CO₂ into fuels: Perspective and challenges. *Renew. Sustain. Energy Rev.* **2019**, *115*, 109333. [[CrossRef](#)]
123. Yadav, D.K.; Singh, D.K.; Ganesan, V. Recent strategy(ies) for the electrocatalytic reduction of CO₂: Ni single-atom catalysts for the selective electrochemical formation of CO in aqueous electrolytes. *Curr. Opin. Electrochem.* **2020**, *22*, 87–93. [[CrossRef](#)]
124. Guo, W.; Shim, K.; Odongo Ngome, F.O.; Moon, Y.H.; Choi, S.-Y.; Kim, Y.-T. Highly active coral-like porous silver for electrochemical reduction of CO₂ to CO. *Appl. Surf. Sci.* **2020**, *41*, 101242. [[CrossRef](#)]
125. Guo, C.; Zhang, T.; Liang, X.; Deng, X.; Guo, W.; Wang, Z.; Lu, X.; Wu, C.-M.L. Single transition metal atoms on nitrogen-doped carbon for CO₂ electrocatalytic reduction: CO production or further CO reduction? *Appl. Surf. Sci.* **2020**, *533*, 147466. [[CrossRef](#)]
126. Guo, W.; Shim, K.; Kim, Y.-T. Ag layer deposited on Zn by physical vapor deposition with enhanced CO selectivity for electrochemical CO₂ reduction. *Appl. Surf. Sci.* **2020**, *526*, 146651. [[CrossRef](#)]
127. Tahir, B.; Tahir, M.; Nawawi, M.G.M. Highly stable 3D/2D WO₃/g-C₃N₄ Z-scheme heterojunction for stimulating photocatalytic CO₂ reduction by H₂O/H₂ to CO and CH₄ under visible light. *J. CO₂ Util.* **2020**, *41*, 101270. [[CrossRef](#)]
128. Kazemi Movahed, S.; Najinasab, A.; Nikbakht, R.; Dabiri, M. Visible light assisted photocatalytic reduction of CO₂ to methanol using Fe₃O₄@N-C/Cu₂O nanostructure photocatalyst. *J. Photochem. Photobiol. A Chem.* **2020**, *401*, 112763. [[CrossRef](#)]
129. Jiang, X.X.; De Hu, X.; Tarek, M.; Saravanan, P.; Alqadhi, R.; Chin, S.Y.; Rahman Khan, M.M. Tailoring the properties of g-C₃N₄ with CuO for enhanced photoelectrocatalytic CO₂ reduction to methanol. *J. CO₂ Util.* **2020**, *40*, 101222. [[CrossRef](#)]
130. Aranda-Aguirre, A.; Ojeda, J.; Ferreira de Brito, J.; Garcia-Segura, S.; Boldrin Zanoni, M.V.; Alarcon, H. Photoelectrodes of Cu₂O with interfacial structure of topological insulator Bi₂Se₃ contributes to selective photoelectrocatalytic reduction of CO₂ towards methanol. *J. CO₂ Util.* **2020**, *39*, 101154. [[CrossRef](#)]
131. Karim, K.M.R.; Tarek, M.; Sarkar, S.M.; Mouras, R.; Ong, H.R.; Abdullah, H.; Cheng, C.K.; Khan, M.M.R. Photoelectrocatalytic reduction of CO₂ to methanol over CuFe₂O₄@PANI photocathode. *Int. J. Hydrog. Energy* **2020**. [[CrossRef](#)]

132. Huang, W.; Yuan, G. A composite heterogeneous catalyst C-Py-Sn-Zn for selective electrochemical reduction of CO₂ to methanol. *Electrochem. Commun.* **2020**, *118*, 106789. [[CrossRef](#)]
133. Cheng, J.; Yang, X.; Xuan, X.; Liu, N.; Zhou, J. Development of an efficient catalyst with controlled sulfur vacancies and high pyridine nitrogen content for the photoelectrochemical reduction of CO₂ into methanol. *Sci. Total Environ.* **2020**, *702*, 134981. [[CrossRef](#)]
134. Liu, Y.; Li, F.; Zhang, X.; Ji, X. Recent progress on electrochemical reduction of CO₂ to methanol. *Curr. Opin. Green Sustain. Chem.* **2020**, *23*, 10–17. [[CrossRef](#)]
135. Tarek, M.; Rezaul Karim, K.M.; Sarkar, S.M.; Deb, A.; Ong, H.R.; Abdullah, H.; Cheng, C.K.; Rahman Khan, M.M. Hetero-structure CdS–CuFe₂O₄ as an efficient visible light active photocatalyst for photoelectrochemical reduction of CO₂ to methanol. *Int. J. Hydrogen Energy* **2019**, *44*, 26271–26284. [[CrossRef](#)]
136. Feng, S.; Zhao, J.; Bai, Y.; Liang, X.; Wang, T.; Wang, C. Facile synthesis of Mo-doped TiO₂ for selective photocatalytic CO₂ reduction to methane: Promoted H₂O dissociation by Mo doping. *J. CO₂ Util.* **2020**, *38*, 1–9. [[CrossRef](#)]
137. Merino-Garcia, I.; Albo, J.; Solla-Gullón, J.; Montiel, V.; Irabien, A. Cu oxide/ZnO-based surfaces for a selective ethylene production from gas-phase CO₂ electroconversion. *J. CO₂ Util.* **2019**, *31*, 135–142. [[CrossRef](#)]
138. Qin, T.; Qian, Y.; Zhang, F.; Lin, B.-L. Chloride-derived copper electrode for efficient electrochemical reduction of CO₂ to ethylene. *Chin. Chem. Lett.* **2019**, *30*, 314–318. [[CrossRef](#)]
139. Fan, L.; Xia, C.; Zhu, P.; Lu, Y.; Wang, H. Electrochemical CO₂ reduction to high-concentration pure formic acid solutions in an all-solid-state reactor. *Nat. Commun.* **2020**, *11*, 3633. [[CrossRef](#)]
140. Zhao, Y.; Wang, T.; Wang, Y.; Hao, R.; Wang, H.; Han, Y. Catalytic reduction of CO₂ to HCO₂[−] by nanoscale nickel-based bimetallic alloy under atmospheric pressure. *J. Ind. Eng. Chem.* **2019**, *77*, 291–302. [[CrossRef](#)]
141. Li, P.; Liu, L.; An, W.; Wang, H.; Guo, H.; Liang, Y.; Cui, W. Ultrathin porous g-C₃N₄ nanosheets modified with AuCu alloy nanoparticles and C-C coupling photothermal catalytic reduction of CO₂ to ethanol. *Appl. Catal. B Environ.* **2020**, *266*, 118618. [[CrossRef](#)]
142. Tekalgne, M.A.; Do, H.H.; Hasani, A.; Van Le, Q.; Jang, H.W.; Ahn, S.H.; Kim, S.Y. Two-dimensional materials and metal-organic frameworks for the CO₂ reduction reaction. *Mater. Today Adv.* **2020**, *5*, 100038. [[CrossRef](#)]
143. Billo, T.; Shown, I.; Anbalagan, A.k.; Effendi, T.A.; Sabbah, A.; Fu, F.-Y.; Chu, C.-M.; Woon, W.-Y.; Chen, R.-S.; Lee, C.-H.; et al. A mechanistic study of molecular CO₂ interaction and adsorption on carbon implanted SnS₂ thin film for photocatalytic CO₂ reduction activity. *Nano Energy* **2020**, *72*, 104717. [[CrossRef](#)]
144. Mu, Q.; Zhu, W.; Li, X.; Zhang, C.; Su, Y.; Lian, Y.; Qi, P.; Deng, Z.; Zhang, D.; Wang, S.; et al. Electrostatic charge transfer for boosting the photocatalytic CO₂ reduction on metal centers of 2D MOF/rGO heterostructure. *Appl. Catal. B Environ.* **2020**, *262*, 118144. [[CrossRef](#)]
145. Ješić, D.; Lašić Jurković, D.; Pohar, A.; Suhadolnik, L.; Likozar, B. Engineering Photocatalytic and Photoelectrocatalytic CO₂ Reduction Reactions: Mechanisms, Intrinsic Kinetics, Mass Transfer Resistances, Reactors and Multi-scale Modelling Simulations. *Chem. Eng. J.* **2020**, 126799. [[CrossRef](#)]
146. Omar, S.; Shkir, M.; Ajmal Khan, M.; Ahmad, Z.; AlFaify, S. A comprehensive study on molecular geometry, optical, HOMO-LUMO, and nonlinear properties of 1,3-diphenyl-2-propen-1-ones chalcone and its derivatives for optoelectronic applications: A computational approach. *Optik* **2020**, *204*, 164172. [[CrossRef](#)]
147. Reddy, C.V.; Reddy, K.R.; Harish, V.V.N.; Shim, J.; Shankar, M.V.; Shetti, N.P.; Aminabhavi, T.M. Metal-organic frameworks (MOFs)-based efficient heterogeneous photocatalysts: Synthesis, properties and its applications in photocatalytic hydrogen generation, CO₂ reduction and photodegradation of organic dyes. *Int. J. Hydrog. Energy* **2020**, *45*, 7656–7679. [[CrossRef](#)]
148. Wang, C.-C.; Zhang, Y.-Q.; Li, J.; Wang, P. Photocatalytic CO₂ reduction in metal–organic frameworks: A mini review. *J. Mol. Struct.* **2015**, *1083*, 127–136. [[CrossRef](#)]
149. Wang, C.; Xie, Z.; deKrafft, K.E.; Lin, W. Doping Metal–Organic Frameworks for Water Oxidation, Carbon Dioxide Reduction, and Organic Photocatalysis. *J. Am. Chem. Soc.* **2011**, *133*, 13445–13454. [[CrossRef](#)]
150. Liu, Q.; Low, Z.-X.; Li, L.; Razmjou, A.; Wang, K.; Yao, J.; Wang, H. ZIF-8/Zn₂GeO₄ nanorods with an enhanced CO₂ adsorption property in an aqueous medium for photocatalytic synthesis of liquid fuel. *J. Mater. Chem. A* **2013**, *1*, 11563–11569. [[CrossRef](#)]
151. Fu, Y.; Sun, D.; Chen, Y.; Huang, R.; Ding, Z.; Fu, X.; Li, Z. An Amine-Functionalized Titanium Metal–Organic Framework Photocatalyst with Visible-Light-Induced Activity for CO₂ Reduction. *Angew. Chem. Int. Ed.* **2012**, *51*, 3364–3367. [[CrossRef](#)] [[PubMed](#)]

152. Li, R.; Hu, J.; Deng, M.; Wang, H.; Wang, X.; Hu, Y.; Jiang, H.L.; Jiang, J.; Zhang, Q.; Xie, Y.; et al. Integration of an inorganic semiconductor with a metal-organic framework: A platform for enhanced gaseous photocatalytic reactions. *Adv. Mater.* **2014**, *26*, 4783–4788. [[CrossRef](#)]
153. Liu, Y.; Yang, Y.; Sun, Q.; Wang, Z.; Huang, B.; Dai, Y.; Qin, X.; Zhang, X. Chemical Adsorption Enhanced CO₂ Capture and Photoreduction over a Copper Porphyrin Based Metal Organic Framework. *ACS Appl. Mater. Interfaces* **2013**, *5*, 7654–7658. [[CrossRef](#)] [[PubMed](#)]
154. Sun, D.; Liu, W.; Fu, Y.; Fang, Z.; Sun, F.; Fu, X.; Zhang, Y.; Li, Z. Noble Metals Can Have Different Effects on Photocatalysis Over Metal–Organic Frameworks (MOFs): A Case Study on M/NH₂-MIL-125(Ti) (M=Pt and Au). *Chem. A Eur. J.* **2014**, *20*, 4780–4788. [[CrossRef](#)]
155. Sun, D.; Liu, W.; Qiu, M.; Zhang, Y.; Li, Z. Introduction of a mediator for enhancing photocatalytic performance via post-synthetic metal exchange in metal–organic frameworks (MOFs). *Chem. Commun.* **2015**, *51*, 2056–2059. [[CrossRef](#)] [[PubMed](#)]
156. Lee, Y.; Kim, S.; Fei, H.; Kang, J.K.; Cohen, S.M. Photocatalytic CO₂ reduction using visible light by metal-monocatecholato species in a metal–organic framework. *Chem. Commun.* **2015**, *51*, 16549–16552. [[CrossRef](#)]
157. Wang, S.; Wang, X. Photocatalytic CO₂ reduction by CdS promoted with a zeolitic imidazolate framework. *Appl. Catal. B Environ.* **2015**, *162*, 494–500. [[CrossRef](#)]
158. Wang, M.; Wang, D.; Li, Z. Self-assembly of CPO-27-Mg/TiO₂ nanocomposite with enhanced performance for photocatalytic CO₂ reduction. *Appl. Catal. B Environ.* **2016**, *183*, 47–52. [[CrossRef](#)]
159. Yan, S.; Ouyang, S.; Xu, H.; Zhao, M.; Zhang, X.; Ye, J. Co-ZIF-9/TiO₂ nanostructure for superior CO₂ photoreduction activity. *J. Mater. Chem. A* **2016**, *4*, 15126–15133. [[CrossRef](#)]
160. Sadeghi, N.; Sharifnia, S.; Sheikh Arabi, M. A porphyrin-based metal organic framework for high rate photoreduction of CO₂ to CH₄ in gas phase. *J. CO₂ Util.* **2016**, *16*, 450–457. [[CrossRef](#)]
161. Xu, H.-Q.; Hu, J.; Wang, D.; Li, Z.; Zhang, Q.; Luo, Y.; Yu, S.-H.; Jiang, H.-L. Visible-Light Photoreduction of CO₂ in a Metal–Organic Framework: Boosting Electron–Hole Separation via Electron Trap States. *J. Am. Chem. Soc.* **2015**, *137*, 13440–13443. [[CrossRef](#)]
162. Goyal, S.; Shaharun, M.S.; Kait, C.F.; Abdullah, B.; Ameen, M. Photoreduction of Carbon Dioxide to Methanol over Copper Based Zeolitic Imidazolate Framework-8: A New Generation Photocatalyst. *Catalysts* **2018**, *8*, 581. [[CrossRef](#)]
163. Chen, M.; Han, L.; Zhou, J.; Sun, C.; Hu, C.; Wang, X.; Su, Z. Photoreduction of carbon dioxide under visible light by ultra-small Ag nanoparticles doped into Co-ZIF-9. *Nanotechnology* **2018**, *29*, 284003. [[CrossRef](#)]
164. Han, B.; Ou, X.; Deng, Z.; Song, Y.; Tian, C.; Deng, H.; Xu, Y.-J.; Lin, Z. Nickel Metal–Organic Framework Monolayers for Photoreduction of Diluted CO₂: Metal-Node-Dependent Activity and Selectivity. *Angew. Chem. Int. Ed.* **2018**, *57*, 16811–16815. [[CrossRef](#)]
165. Chen, C.; Wu, T.; Wu, H.; Liu, H.; Qian, Q.; Liu, Z.; Yang, G.; Han, B. Highly effective photoreduction of CO₂ to CO promoted by integration of CdS with molecular redox catalysts through metal–organic frameworks. *Chem. Sci.* **2018**, *9*, 8890–8894. [[CrossRef](#)]
166. Sadeghi, N.; Sharifnia, S.; Do, T.-O. Enhanced CO₂ photoreduction by a graphene–porphyrin metal–organic framework under visible light irradiation. *J. Mater. Chem. A* **2018**, *6*, 18031–18035. [[CrossRef](#)]
167. Ye, L.; Gao, Y.; Cao, S.; Chen, H.; Yao, Y.; Hou, J.; Sun, L. Assembly of highly efficient photocatalytic CO₂ conversion systems with ultrathin two-dimensional metal–organic framework nanosheets. *Appl. Catal. B Environ.* **2018**, *227*, 54–60. [[CrossRef](#)]
168. Li, D.; Kassymova, M.; Cai, X.; Zang, S.-Q.; Jiang, H.-L. Photocatalytic CO₂ reduction over metal-organic framework-based materials. *Coord. Chem. Rev.* **2020**, *412*, 213262. [[CrossRef](#)]
169. Li, P.-Z.; Wang, X.-J.; Liu, J.; Phang, H.S.; Li, Y.; Zhao, Y. Highly Effective Carbon Fixation via Catalytic Conversion of CO₂ by an Acylamide-Containing Metal–Organic Framework. *Chem. Mater.* **2017**, *29*, 9256–9261. [[CrossRef](#)]
170. Ding, D.; Jiang, Z.; Jin, J.; Li, J.; Ji, D.; Zhang, Y.; Zan, L. Impregnation of semiconductor CdS NPs in MOFs cavities via double solvent method for effective photocatalytic CO₂ conversion. *J. Catal.* **2019**, *375*, 21–31. [[CrossRef](#)]
171. Li, X.; Zhu, Q.-L. MOF-based materials for photo- and electrocatalytic CO₂ reduction. *EnergyChem* **2020**, *2*, 100033. [[CrossRef](#)]

172. Wang, L.; Jin, P.; Duan, S.; She, H.; Huang, J.; Wang, Q. In-situ incorporation of Copper(II) porphyrin functionalized zirconium MOF and TiO₂ for efficient photocatalytic CO₂ reduction. *Sci. Bull.* **2019**, *64*, 926–933. [[CrossRef](#)]
173. Dong, H.; Zhang, X.; Lu, Y.; Yang, Y.; Zhang, Y.-P.; Tang, H.-L.; Zhang, F.-M.; Yang, Z.-D.; Sun, X.; Feng, Y. Regulation of metal ions in smart metal-cluster nodes of metal-organic frameworks with open metal sites for improved photocatalytic CO₂ reduction reaction. *Appl. Catal. B Environ.* **2020**, *276*, 119173. [[CrossRef](#)]
174. Chen, S.; Yu, J.; Zhang, J. Enhanced photocatalytic CO₂ reduction activity of MOF-derived ZnO/NiO porous hollow spheres. *J. CO₂ Util.* **2018**, *24*, 548–554. [[CrossRef](#)]
175. Crake, A.; Christoforidis, K.C.; Kafizas, A.; Zafeiratos, S.; Petit, C. CO₂ capture and photocatalytic reduction using bifunctional TiO₂/MOF nanocomposites under UV-vis irradiation. *Appl. Catal. B Environ.* **2017**, *210*, 131–140. [[CrossRef](#)]
176. Ma, Z.; Wu, D.; Han, X.; Wang, H.; Zhang, L.; Gao, Z.; Xu, F.; Jiang, K. Ultrasonic assisted synthesis of Zn-Ni bi-metal MOFs for interconnected Ni-N-C materials with enhanced electrochemical reduction of CO₂. *J. CO₂ Util.* **2019**, *32*, 251–258. [[CrossRef](#)]
177. Kang, X.; Gollan, R.J.; Jacobs, P.A.; Veeraragavan, A. Suppression of instabilities in a premixed methane-air flame in a narrow channel via hydrogen/carbon monoxide addition. *Combust. Flame* **2016**, *173*, 266–275. [[CrossRef](#)]
178. Wang, Y.-R.; Huang, Q.; He, C.-T.; Chen, Y.; Liu, J.; Shen, F.-C.; Lan, Y.-Q. Oriented electron transmission in polyoxometalate-metalloporphyrin organic framework for highly selective electroreduction of CO₂. *Nat. Commun.* **2018**, *9*, 4466. [[CrossRef](#)]
179. Ye, L.; Liu, J.; Gao, Y.; Gong, C.; Addicoat, M.; Heine, T.; Wöll, C.; Sun, L. Highly oriented MOF thin film-based electrocatalytic device for the reduction of CO₂ to CO exhibiting high faradaic efficiency. *J. Mater. Chem. A* **2016**, *4*, 15320–15326. [[CrossRef](#)]
180. Wang, Y.; Hou, P.; Wang, Z.; Kang, P. Zinc Imidazolate Metal-Organic Frameworks (ZIF-8) for Electrochemical Reduction of CO₂ to CO. *ChemPhysChem* **2017**, *18*, 3142–3147. [[CrossRef](#)] [[PubMed](#)]
181. Guo, Y.; Yang, H.; Zhou, X.; Liu, K.; Zhang, C.; Zhou, Z.; Wang, C.; Lin, W. Electrocatalytic reduction of CO₂ to CO with 100% faradaic efficiency by using pyrolyzed zeolitic imidazolate frameworks supported on carbon nanotube networks. *J. Mater. Chem. A* **2017**, *5*, 24867–24873. [[CrossRef](#)]
182. Kornienko, N.; Zhao, Y.; Kley, C.S.; Zhu, C.; Kim, D.; Lin, S.; Chang, C.J.; Yaghi, O.M.; Yang, P. Metal-Organic Frameworks for Electrocatalytic Reduction of Carbon Dioxide. *J. Am. Chem. Soc.* **2015**, *137*, 14129–14135. [[CrossRef](#)]
183. Hinogami, R.; Yotsuhashi, S.; Deguchi, M.; Zenitani, Y.; Hashiba, H.; Yamada, Y. Electrochemical Reduction of Carbon Dioxide Using a Copper Rubenate Metal Organic Framework. *ECS Electrochem. Lett.* **2012**, *1*, H17–H19. [[CrossRef](#)]
184. Perfecto-Irigaray, M.; Albo, J.; Beobide, G.; Castillo, O.; Irabien, A.; Pérez-Yáñez, S. Synthesis of heterometallic metal-organic frameworks and their performance as electrocatalyst for CO₂ reduction. *RSC Adv.* **2018**, *8*, 21092–21099. [[CrossRef](#)]
185. Ye, Y.; Cai, F.; Li, H.; Wu, H.; Wang, G.; Li, Y.; Miao, S.; Xie, S.; Si, R.; Wang, J.; et al. Surface functionalization of ZIF-8 with ammonium ferric citrate toward high exposure of Fe-N active sites for efficient oxygen and carbon dioxide electroreduction. *Nano Energy* **2017**, *38*, 281–289. [[CrossRef](#)]
186. Huan, T.N.; Ranjbar, N.; Rouse, G.; Sougrati, M.; Zitolo, A.; Mougél, V.; Jaouen, F.; Fontecave, M. Electrochemical Reduction of CO₂ Catalyzed by Fe-N-C Materials: A Structure-Selectivity Study. *ACS Catal.* **2017**, *7*, 1520–1525. [[CrossRef](#)]
187. Tan, X.; Yu, C.; Zhao, C.; Huang, H.; Yao, X.; Han, X.; Guo, W.; Cui, S.; Huang, H.; Qiu, J. Restructuring of Cu₂O to Cu₂O@Cu-Metal-Organic Frameworks for Selective Electrochemical Reduction of CO₂. *ACS Appl. Mater. Interfaces* **2019**, *11*, 9904–9910. [[CrossRef](#)]
188. Li, F.; Gu, G.H.; Choi, C.; Kolla, P.; Hong, S.; Wu, T.-S.; Soo, Y.-L.; Masa, J.; Mukerjee, S.; Jung, Y.; et al. Highly stable two-dimensional bismuth metal-organic frameworks for efficient electrochemical reduction of CO₂. *Appl. Catal. B Environ.* **2020**, *277*, 119241. [[CrossRef](#)]
189. Rayer, A.V.; Reid, E.; Kataria, A.; Luz, I.; Thompson, S.J.; Lail, M.; Zhou, J.; Soukri, M. Electrochemical carbon dioxide reduction to isopropanol using novel carbonized copper metal organic framework derived electrodes. *J. CO₂ Util.* **2020**, *39*, 101159. [[CrossRef](#)]

190. Zhang, S.-Y.; Yang, Y.-Y.; Zheng, Y.-Q.; Zhu, H.-L. Ag-doped Co₃O₄ catalyst derived from heterometallic MOF for syngas production by electrocatalytic reduction of CO₂ in water. *J. Solid State Chem.* **2018**, *263*, 44–51. [[CrossRef](#)]
191. Cao, S.-M.; Chen, H.-B.; Dong, B.-X.; Zheng, Q.-H.; Ding, Y.-X.; Liu, M.-J.; Qian, S.-L.; Teng, Y.-L.; Li, Z.-W.; Liu, W.-L. Nitrogen-rich metal-organic framework mediated Cu–N–C composite catalysts for the electrochemical reduction of CO₂. *J. Energy Chem.* **2021**, *54*, 555–563. [[CrossRef](#)]
192. Sun, X.; Wang, R.; Ould-Chikh, S.; Osadchii, D.; Li, G.; Aguilar, A.; Hazemann, J.-I.; Kapteijn, F.; Gascon, J. Structure-activity relationships in metal organic framework derived mesoporous nitrogen-doped carbon containing atomically dispersed iron sites for CO₂ electrochemical reduction. *J. Catal.* **2019**, *378*, 320–330. [[CrossRef](#)]
193. Al-Rowaili, F.N.; Jamal, A.; Ba Shammakh, M.S.; Rana, A. A Review on Recent Advances for Electrochemical Reduction of Carbon Dioxide to Methanol Using Metal–Organic Framework (MOF) and Non-MOF Catalysts: Challenges and Future Prospects. *Acs Sustain. Chem. Eng.* **2018**, *6*, 15895–15914. [[CrossRef](#)]
194. Dong, B.-X.; Qian, S.-L.; Bu, F.-Y.; Wu, Y.-C.; Feng, L.-G.; Teng, Y.-L.; Liu, W.-L.; Li, Z.-W. Electrochemical Reduction of CO₂ to CO by a Heterogeneous Catalyst of Fe–Porphyrin-Based Metal–Organic Framework. *ACS Appl. Energy Mater.* **2018**, *1*, 4662–4669. [[CrossRef](#)]
195. Hod, I.; Sampson, M.D.; Deria, P.; Kubiak, C.P.; Farha, O.K.; Hupp, J.T. Fe-Porphyrin-Based Metal–Organic Framework Films as High-Surface Concentration, Heterogeneous Catalysts for Electrochemical Reduction of CO₂. *ACS Catal.* **2015**, *5*, 6302–6309. [[CrossRef](#)]
196. Wang, R.; Sun, X.; Ould-Chikh, S.; Osadchii, D.; Bai, F.; Kapteijn, F.; Gascon, J. Metal-Organic-Framework-Mediated Nitrogen-Doped Carbon for CO₂ Electrochemical Reduction. *ACS Appl. Mater. Interfaces* **2018**, *10*, 14751–14758. [[CrossRef](#)]
197. Witman, M.; Ling, S.; Gladysiak, A.; Stylianou, K.C.; Smit, B.; Slater, B.; Haranczyk, M. Rational Design of a Low-Cost, High-Performance Metal–Organic Framework for Hydrogen Storage and Carbon Capture. *J. Phys. Chem. C* **2017**, *121*, 1171–1181. [[CrossRef](#)] [[PubMed](#)]
198. DeSantis, D.; Mason, J.A.; James, B.D.; Houchins, C.; Long, J.R.; Veenstra, M. Techno-economic Analysis of Metal–Organic Frameworks for Hydrogen and Natural Gas Storage. *Energy Fuels* **2017**, *31*, 2024–2032. [[CrossRef](#)]

Publisher’s Note: MDPI stays neutral with regard to jurisdictional claims in published maps and institutional affiliations.



© 2020 by the authors. Licensee MDPI, Basel, Switzerland. This article is an open access article distributed under the terms and conditions of the Creative Commons Attribution (CC BY) license (<http://creativecommons.org/licenses/by/4.0/>).